JGR Oceans

RESEARCH ARTICLE
10.1029/2021JC017424

Special Section:
Uncovering the hidden links between dynamics, chemical, biogeochemical and biological processes under the changing Arctic

Summer Surface CO_2 Dynamics on the Bering Sea and Eastern Chukchi Sea Shelves From 1989 to 2019

Hongjie Wang[1,2], Peigen Lin[3], Robert S. Pickart[3], and Jessica N. Cross[2]

[1]University of Washington Cooperative Institute for Climate, Ocean, and Ecosystem Science, Seattle, WA, USA, [2]NOAA Pacific Marine Environmental Laboratory, Seattle, WA, USA, [3]Woods Hole Oceanographic Institution, Woods Hole, MA, USA

Abstract By compiling boreal summer (June to October) CO_2 measurements from 1989 to 2019 on the Bering and eastern Chukchi Sea shelves, we find that the study areas act as a CO_2 sink except when impacted by river runoff and wind-driven upwelling. The CO_2 system in this area is seasonally dominated by the biological pump especially in the northern Bering Sea and near Hanna Shoal, while wind-driven upwelling of CO_2-rich bottom water can cause episodic outgassing. Seasonal surface ΔfCO_2 (oceanic fCO_2 – air fCO_2) is dominantly driven by temperature only during periods of weak CO_2 outgassing in shallow nearshore areas. However, after comparing the mean summer ΔfCO_2 during the periods of 1989–2013 and 2014–2019, we suggest that temperature does drive long-term, multi-decadal patterns in ΔfCO_2. In the northern Chukchi Sea, rapid warming concurrent with reduced seasonal sea-ice persistence caused the regional summer CO_2 sink to decrease. By contrast, increasing primary productivity caused the regional summer CO_2 sink on the Bering Sea shelf to increase over time. While additional time series are needed to confirm the seasonal and annual trajectory of CO_2 changes and ocean acidification in these dynamic and spatially complex ecosystems, this study provides a meaningful mechanistic analysis of recent changes in inorganic carbonate chemistry. As high-resolution time series of inorganic carbonate parameters lengthen and short-term variations are better constrained in the coming decades, we will have stronger confidence in assessing the mechanisms contributing to long-term changes in the source/sink status of regional sub-Arctic seas.

Plain Language Summary The ocean performs an essential function for the planet by removing carbon dioxide (CO_2) from the atmosphere, providing an important limit on climate change and global warming. Hence it is critical to understand how much CO_2 can be absorbed by the ocean surface in different regions and at different times of the year. On the Bering and Chukchi Sea shelves, ocean plants and temperature control how much CO_2 can be absorbed by the ocean, especially during summer (June to October), and both are changing as our climate warms. Using 30 years of field data, we find that, on average, ocean plants help take up a substantial amount of CO_2 on the shelves during summer. Over time, ocean plants on the Bering Sea shelf have been taking up more and more CO_2 each summer; however, on the Chukchi Sea shelf, warming ocean temperatures have resulted in less CO_2 uptake each summer. While our study shows that climate change can impact CO_2 uptake by changing ocean temperatures and ocean plant activity, it is unclear if these changes are permanent or temporary. More data and research are essential to better understand these trends.

Key Points:

- The Bering and eastern Chukchi Sea shelves act as summer CO_2 sinks, except when impacted by river runoff and wind-driven overturning
- The summer surface CO_2 is driven by primary productivity, while summer warming is only apparent in shallow nearshore areas
- Rapid summer warming decreased the Chukchi sea shelf CO_2 sink, while increasing primary productivity increased the Bering Sea shelf CO_2 sink

Supporting Information:

Supporting Information may be found in the online version of this article.

Correspondence to:

H. Wang and P. Lin,
hwang@uri.edu;
plin@whoi.edu

Citation:

Wang, H., Lin, P., Pickart, R. S., & Cross, J. N. (2022). Summer surface CO_2 dynamics on the Bering Sea and eastern Chukchi Sea shelves from 1989 to 2019. *Journal of Geophysical Research: Oceans*, *127*, e2021JC017424. https://doi.org/10.1029/2021JC017424

Received 1 APR 2021
Accepted 26 NOV 2021

Author Contributions:

Conceptualization: Hongjie Wang, Peigen Lin, Robert S. Pickart, Jessica N. Cross
Formal analysis: Hongjie Wang, Peigen Lin
Funding acquisition: Robert S. Pickart, Jessica N. Cross
Methodology: Hongjie Wang, Robert S. Pickart, Jessica N. Cross

1. Introduction

Human activities have increased the atmospheric CO_2 concentrations from ~280 μatm before the Industrial Revolution to ~410 μatm in 2020. The continuous dissolution of anthropogenic CO_2 has lowered global ocean pH by ~0.1, a process commonly known as ocean acidification (OA, Orr et al., 2005). OA can be more rapid and intensified in some hotspots because of regional biogeochemical processes. In the North Pacific and Pacific Arctic, these exacerbations can include mechanisms such as coastal upwelling (Feely et al., 2008), glacial melt (Evans et al., 2014; Jones et al., 2017; Pilcher et al., 2018), river runoff (Cross et al., 2013; D'Olivo et al., 2013; Mathis et al., 2011b, 2011a; Polukhin, 2019), the biological pump (Cross, Mathis, Frey, et al., 2014; Cross, Mathis, Lomas, et al., 2014; Cross et al., 2018), and eutrophication (Cai et al., 2011). Given this natural vulnerability and anthropogenic acidification, the volume of undersaturated water (calcium carbonate saturation state <1) in the Pacific halocline is expanding northwards to the Arctic Ocean (Qi et al., 2017). Terhaar et al. (2020) recently reported that a basin-averaged undersaturated state would be reached before the end of 21st century. Some

Supervision: Robert S. Pickart, Jessica N. Cross
Visualization: Hongjie Wang, Peigen Lin
Writing – original draft: Hongjie Wang, Peigen Lin
Writing – review & editing: Hongjie Wang, Peigen Lin, Robert S. Pickart, Jessica N. Cross

impacts of this acidification can already be detected: for example, the combination of anthropogenic CO_2 uptake and natural processes can result in seasonal carbonate mineral dissolution in the Bering Sea (Cross et al., 2013).

Despite many efforts investigating the carbonate system in high-latitude areas, there remains considerable uncertainty regarding sea-air CO_2 fluxes. For example, estimates of the Arctic Ocean CO_2 flux can range from −1 to −20 mmol C m^{-2} d^{-1} (from atmosphere to ocean), depending on the approach used (Manizza et al., 2019). Similarly, the Bering Sea shelf's annual sea-air CO_2 flux varies from −0.66 to −22 mmol C m^{-2} d^{-1} (Cross, Mathis, Frey et al., 2014; Manizza et al., 2019; Sun et al., 2020). A primary reason for such high flux uncertainty is regional and sub-regional temporal and spatial variability. In many cases, this variability is linked to sea ice: for example, the presence of sea-ice over the southeastern Bering Sea shelf can control the spring phytoplankton bloom and associated CO_2 drawdown, and the extent of ice cover and the timing of retreat vary interannually (Kachel et al., 2002; Sigler et al., 2014). Meanwhile, fall blooms in the Bering Sea and Chukchi Seas are highly variable (Waga & Hirawake, 2020). These changing seasonal influences cause intense variability in sea-air CO_2 fluxes and the overall carbon cycle (Cross, Mathis, Frey, et al., 2014; Cross, Mathis, Lomas, et al., 2014).

In addition to exerting control over phytoplankton production and the biological pump, recent studies have reported that the ice matrix itself can significantly regulate sea-air CO_2 exchange (Geilfus et al., 2013; Rysgaard et al., 2011). In some cases, ice crystal formation increases the gas exchange efficiency through the surface film. Simultaneously, intense supersaturation of carbonates in brine leads to carbonate mineral precipitation (Anderson et al., 2004). The subsequent sea-ice melt during the summer period therefore releases highly buffered meltwater with low $fCO2$ (fugacity of CO_2) back to the surface layer, enhancing the seasonal uptake of atmospheric CO_2 (e.g., Cross et al., 2013; Rysgaard et al., 2009). Moreover, ice algal production reduces surface-water CO_2 concentrations, enhancing the sea-air gas exchange through the ice matrix (Rysgaard et al., 2007, 2011). The combined influence of all these processes as well as physical conditions during ice formation and melt can substantially moderate how gas moves through the ice matrix, and the influence that ice melt can have on the ocean surface (Bates et al., 2014).

There is a general agreement among the scientific community that sea ice is expected to become thinner, younger, and more ephemeral as the Arctic system continues to warm (Lannuzel et al., 2020). However, there is an ongoing debate about the response of the carbon system to continued sea-ice loss. On one hand, increasing open water area favors oceanic uptake of CO_2 by allowing more light penetration to enhance productivity and by removing the mechanical barrier for sea-air CO_2 exchange (Arrigo et al., 2008; Arrigo & van Dijken, 2015; Bates et al., 2006; Bates & Mathis, 2009; Lewis et al., 2020). However, meltwater can also increase surface stratification, which limits the ocean's capacity for surface storage of CO_2, suppresses nutrient replenishment from depth, and depresses the efficiency of biological carbon pump (Cai et al., 2010; DeGrandpre et al., 2020; Lannuzel et al., 2020; Ouyang et al., 2020). Further nuance results from ongoing warming that favors permafrost thaw and changes the riverine and groundwater flux of carbon and nutrients to Alaskan waters (Schuur et al., 2015; Tank et al., 2016; Vonk et al., 2015; Walvoord & Striegl, 2007). The photochemical degradation of terrigenous material can also make the terrestrial dissolved organic carbon labile for microbial respiration (Ward et al., 2014, 2017). All the processes mentioned above make it challenging to predict changes in the carbon system at high latitudes as the regional impacts of climate continue to emerge (Lannuzel et al., 2020).

In this study, we use the Surface Oceanic CO_2 Atlas version 2020 (SOCATv2020) combined with an extensive new dataset of surface ocean carbon measurements collected from autonomous platforms to examine both the spatial and temporal changes of summer (June to October) surface fCO_2 over the Bering and Chukchi Sea shelves from 1989 to 2019. First, we explore the mechanisms that influence summer surface fCO_2 dynamics, including temperature, the biological carbon pump, and ocean circulation. We then discuss the change in summer fCO_2 as the system has warmed over time. Last, we address the underlying processes controlling the changes in summer fCO_2 over time. This study's analysis of summer fCO_2 long-term change is essential to predicting changes in the carbon cycle in a warm, low-ice future.

2. Study Area

The Bering and Chukchi Seas are shallow (water depths <150 m) continental shelves that represent the gateway from the North Pacific Ocean to the Arctic Ocean (Figure 1). The water masses and circulation in the study area have been addressed by many previous studies (e.g., Lin, Pickart, McRaven et al., 2019; Lin, Pickart, Moore,

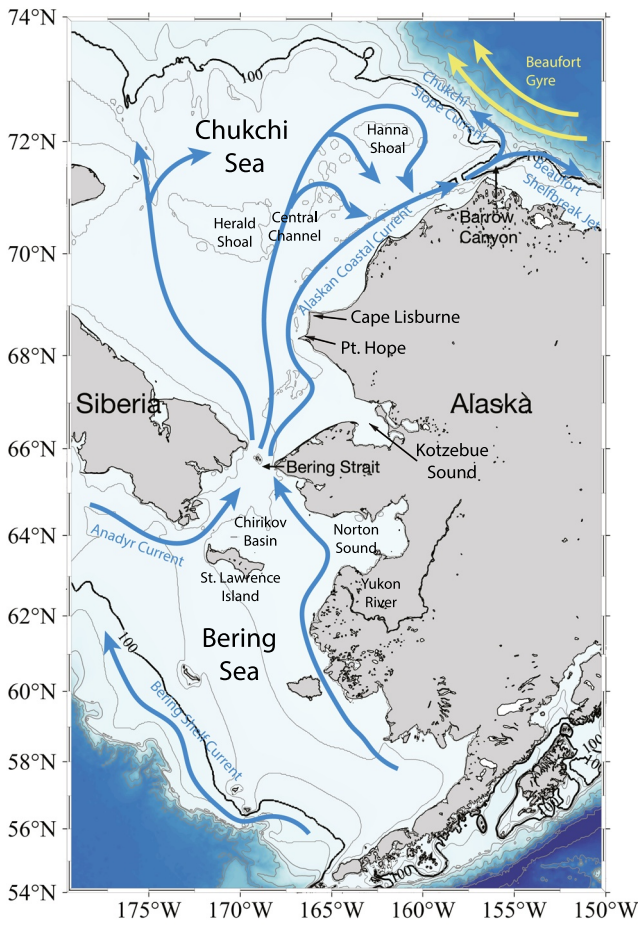

Figure 1. Schematic circulation map with geographic place names. The shaded bathymetry is from 2-min Gridded Global Relief Data (ETOPO2, 2006).

et al., 2019; Pickart et al., 2019). Here, we briefly review a few of the known features in the study area to facilitate later discussion.

In the Bering Sea, the timing and extent of seasonal sea ice play important roles in determining the physical and biological structure of the water column (Ladd & Stabeno, 2012), but the combination of wind-driven and tidal mixing with bottom topography generally leads to the formation of three along-shelf domains separated by semi-permanent frontal structures at the 50 and 100 m isobaths (Kachel et al., 2002; Schumacher et al., 1979; Stabeno et al., 1999). The Coastal Domain (coast to ~50 m isobath) is often unstratified due to mixing of the upper and lower portions of the water column by wind and tides, respectively, although freshwater discharge during the start of spring can cause some ephemeral stratification. As the shelf deepens, stratification emerges in the Middle Domain (~50–~100 m water depth) between a dense, tidally mixed bottom layer and a wind-mixed surface layer. The Outer Domain (~100 m water depth to the shelfbreak) also exhibits some stratification, but the pycnocline is often less sharp. Tidal energy controls most of the cross-shelf circulation on the Bering Sea shelf. Slow along-shelf flow (<5 cm s^{-1}) typically follows the bathymetry northward.

Bering Strait, 85 km wide and 50 m deep, is the sole gateway of Pacific water into the western Arctic Ocean. The annual mean current velocities in this narrow, shallow passage range from 20–40 cm s^{-1}, with the strongest mean flow in the western channel (Woodgate, 2018). There are three primary branches in the Bering Strait inflow. The Alaskan Coastal Current (ACC) flows northward on the eastern side of the strait along the coast toward Barrow Canyon. The ACC advects warm, fresh, nutrient-poor Alaskan Coastal Water (ACW, Table 1), mainly during summer, which originates from continental runoff (Stabeno et al., 1995; Woodgate et al., 2015). On the western side of the strait is the northward extension of the Anadyr Current (Stabeno et al., 2016) which flows along the Siberian coast and transports nutrient-rich Anadyr Water (Mordy et al., 2020). Flow from the central Bering Sea shelf forms the central branch of the throughflow (Stabeno et al., 2018).

Anadyr water and central Bering shelf water mix to the north of Bering Strait and are often collectively referred to as Bering Summer Water (BSW, Table 1, Lin, Pichart, Moore, et al., 2019). BSW is typically slightly saltier than ACW since it is not influenced by freshwater inputs, and contains low O_2, high CO_2, and relatively high nutrient concentrations accumulated from remineralization of sinking particles on the Bering shelf (Cross et al., 2018; Grebmeier et al., 2015). North of Bering Strait, BSW flows poleward through Herald Canyon (Linders et al., 2017) and through the Central Channel between Herald and Hanna Shoals (Gong & Pickart, 2015). A portion of the central channel flow bifurcates to the east prior to approaching Hanna Shoal, while the remainder progresses northward and flows clockwise around the shoal (Lin, Pickart, McRaven et al., 2019; Lin, Pickart, Moore, et al., 2019; Pickart et al., 2016). These two branches converge southeast of the shoal and eventually join the ACC, which subsequently flows off the shelf through Barrow Canyon and contributes to the Beaufort Shelfbreak Jet and Chukchi Slope Current (Figure 1). Very fresh sea-ice meltwater (MW) and river water (RW) can also be found in the Chukchi Sea. The remaining two water masses are Pacific Winter Water and Atlantic Water, rarely measured at the surface, which are not considered in this study. Following previous studies (e.g., Itoh et al., 2015; Lin, Pickart, McRaven et al., 2019; Lin, Pickart, Moore, et al., 2019; Pickart et al., 2016), the water masses are defined in Table 1. Note that the temperature and salinity boundaries are not precise.

Table 1
The Primary Water Masses in the Bering and Chukchi Seas in Summer

Water mass	Abbreviations	Temperature (°C)	Salinity
River water	RW	$T > 8$	$S < 30$
Meltwater	MW	$T < 8$	$S < 30$
Alaskan coastal water	ACW	$T > 3$	$30 < S < 32$
Bering summer water	BSW	$T > 3$	$32 < S < 33.64$
		$0 < T < 3$	$30 < S < 33.64$

3. Data and Methods

3.1. Underway Measurements

Underway measurements of sea surface temperature, salinity and fCO_2 were compiled from SOCATv2020. SOCAT is a quality-controlled surface ocean fCO_2 observational synthesis compiled by the international carbon research community. The accuracy of SOCAT fCO_2 is better than 2 µatm. The sampling frequency is highly variable inside the SOCAT. Most of data collection (individual data points) ranges from 1 to 15 min, while some early data collection ranges from 1 to 3 hr depending on the platforms. Each succeeding version of SOCAT synthesis products contains new data and updates older datasets as necessary. At the time of this analysis, SOCATv2020 was the most up-to-date version available. More information about the SOCAT data product is available from Bakker et al., 2016. Note also that while the fCO_2 records range from 1989 to 2019, the number of annual data points is about one order of magnitude higher in years after 2010 (Figure S1 in Supporting Information S1).

The fCO_2 monthly data density in the study area is highly uneven, with most of the surface fCO_2 collected during the summer open water season (Figure S1 in Supporting Information S1; see also Evans et al., 2015). Thus, in this study, we only focus on the warm season to best avoid sampling biases caused by uneven data coverage. Note that the timing of the seasonal cycle in the Bering and Chukchi Sea shelves do not necessarily correspond. The spring bloom occurs earlier in the Bering Sea than in the Chukchi Sea, owing to earlier ice melt in the Bering Sea. Consequently, the summer arrives in the Bering Sea shelf earlier than the Chukchi Sea shelf. Here, we use summer to represent the calendar period from June to October unless otherwise stated.

We also add the most recent quality-controlled ocean fCO_2 products collected by the saildrone unmanned surface vehicles (USVs), with missions in 2017, 2018 and 2019. Briefly, the saildrone USV is a wind-powered autonomous surface vehicle with a 7 m hull, 5 m wing sail, and 2.5 m keel. The saildrone USVs adopts the same Autonomous Surface Vehicle CO_2 system (ASVCO2) that has previously been packaged for moored autonomous CO_2 systems (MAPCO2, Sutton et al., 2019). Sabine et al. (2020) confirmed that saildrone USVs can robustly collect air and seawater fCO_2 data within ±2 µatm uncertainty based on comparison with NOAA Greenhouse Gas Marine Boundary Layer Reference, ship-board underway systems, and the MAPCO2 system. Here, In each of the three summers, two saildrone USVs were launched from Dutch Harbor, Alaska as part of the Distributed Biological Observatory-Northern Chukchi Integrated Study (DBO-NCIS) sponsored by NOAA's Arctic Research Program, with additional support from the NOAA Ocean Acidification Program and the NOAA Innovative Technology for Arctic Exploration Program. The temporal resolution of fCO_2 measurements from saildrone USVs is hourly. To avoid sampling frequency bias between SOCAT and USVs, we averaged SOCAT fCO_2 data into hourly means in this study.

3.2. Reanalysis Data

To calculate CO_2 flux, we use the 10-m wind fields from the ERA5 reanalysis from the European Center for Medium-Range Weather Forecasts (ECMWF, https://www.ecmwf.int/). ERA5 is the most recent generation of ECMWF reanalysis with a temporal resolution of 1 hr and spatial resolution of 0.25°. Other wind products do not provide temporal resolution on the same scale as our fCO_2 measurements.

To be consistent with the historical fCO_2 data, the annual (12-month) mean sea surface temperature is computed using the ERA5 reanalysis from 1989–2019, which has the same spatial and temporal resolution as the wind products. The data source of the ERA5 sea surface temperature reanalysis includes the Hadley Centre Sea Ice and Sea Surface Temperature data set version 2 (HadISST2, Titchner & Rayner, 2014) prior to September 2007, and the Operational SST and Sea Ice Analysis (OSTIA, Donlon et al., 2012) after September 2007. HadISST2 assimilates in-situ observations as well as two infrared radiometers: the Along Track Scanning Radiometer (ATSR) and the Advanced Very High Resolution Radiometer (AVHRR). OSTIA uses satellite sea surface temperature data provided by international agencies via the Group for High Resolution SST (GHRSST) Regional/Global Task Sharing (R/GTS) framework, and in-situ sea surface temperature data available over the Global Telecommunications System (GTS).

3.3. Satellite Ice Coverage

The satellite-based daily sea-ice concentration used in this analysis is the AVHRR product, obtained from the National Climate Data Center (NODC) of the National Oceanic and Atmospheric Administration (https://psl.noaa.gov/data/gridded/data.noaa.oisst.v2.highres.html). This product is a high-resolution blended analysis of daily ice concentration. It has a spatial grid resolution of 0.25° × 0.25°. To be consistent, we used the data in the time period 1989 to 2019. While cloud cover can cause errors in sea-ice coverage estimates from AVHRR products, especially where low-level clouds and fog have similar temperature or albedo signatures as the surrounding ice, the AVHRR product has been developed using optimum interpolation (e.g., as developed by Reynolds et al., 2007 for blended sea surface temperature analyses) to fill in gaps such as cloud-masked grid cells where low-lying clouds were identifiable. Accordingly, we expect the potential error resulting from cloud cover in the AVHRR product to be minimal.

3.4. Decomposition of Sea-Air CO_2 Differences

ΔfCO_2 (oceanic fCO_2 – air fCO_2) determines the direction of sea-air CO_2 flux: that is, a positive ΔfCO_2 value corresponds to CO_2 source, while a negative value corresponds to CO_2 sink. To explore the drivers of the sea-air CO_2 flux in the study regions, we follow a similar approach to that developed by Takahashi et al. (2002) and calculate the impact of changing sea surface temperature (T) and all other non-thermal processes (nonT) on the observed fCO_2 ocean-atmosphere differences as follows:

$$T(\Delta fCO_2) = fCO_2 - \mathrm{n}fCO_2 \quad (1)$$

$$\mathrm{nonT}(\Delta fCO_2) = \mathrm{n}fCO_2 - fCO_2(\mathrm{atm}) \quad (2)$$

The quantity $nfCO_2$ is the temperature-normalized fCO_2 relative to the climatological mean sea surface temperature (Figure S2 in Supporting Information S1), $nfCO_2 = fCO_2 \times \exp(0.0423\,[T_{mean} - T_{obs}])$ (Takahashi et al., 2002), where T_{obs} is the in-situ temperature, and T_{mean} is the climatological annual mean calculated from the full ERA5 reanalysis from 1989–2019. Thus, Equation 1 is a measure of the temperature effect on the oceanic CO_2 at a given time, relative to the climatological annual mean temperature. fCO_2(atm) was calculated based on the monthly average air CO_2 measured at Mauna Loa and SST and SSS when oceanic fCO_2 was measured. Equation 2 represents the impact of all other processes unrelated to temperature, such as biological CO_2 utilization or production, sea-air exchange of CO_2, sea-ice melt, vertical/lateral transport of CO_2 and alkalinity, and $CaCO_3$ production/dissolution (e.g., Bates et al., 2011; Cross, Mathis, Frey et al., 2014). Previous work has shown consistently that the biological effect, that is, the balance of photosynthesis and respiration, is the most dominant process driving variability in non-thermal processes in this region (Bates et al., 2011; Cross, Mathis, Frey, et al., 2014; Takahashi et al., 2002), far outweighing the other mechanistic contributions.

Note that $T(\Delta fCO_2)$ and $\mathrm{nonT}(\Delta fCO_2)$ in this study are different from the thermal and non-thermal fCO_2 components calculated as Equations 3 and 4 in Takahashi et al. (2002). The latter calculations are designed to study the seasonal variability of oceanic CO_2. In theory, the sum of thermal and non-thermal fCO_2 components from Takahashi et al. (2002) is equal to the seasonal variability at any given sampling time. Thus, the calculations from Takahashi et al. (2002) have a hidden assumption that the annual mean of fCO_2 should be well represented. In high-latitude areas, under-sampling during winter prevents robust estimates of annual mean fCO_2. Since we target the mechanisms that contribute to the seasonal sea-air flux, we chose to use the air fCO_2 as the reference when calculating $\mathrm{nonT}(\Delta fCO_2)$ in this study (Cross, Mathis, Frey, et al., 2014). Accordingly, in our study the sum of $T(\Delta fCO_2)$ and $\mathrm{nonT}(\Delta fCO_2)$ is equal to the ΔfCO_2 at any given sampling time.

4. Spatial Distribution of ΔfCO_2

4.1. Mean State

The summer ΔfCO_2 is generally larger in the Bering Sea shelf (−85 ± 74 μatm) than in the Chukchi Sea shelf (−121 ± 76 μatm). In part, this is due to differences in the timing of the seasonal cycle: much of the spring bloom occurs prior to June in the Bering Sea vs. the Chukchi Sea, owing to earlier ice melt in the Bering Sea. Consequently, the Bering Sea shelf has often entered a period of slowing production or even nutrient limitation in summer while phytoplankton production is peaking in the Chukchi Sea. Overall, the mean surface ΔfCO_2 in the

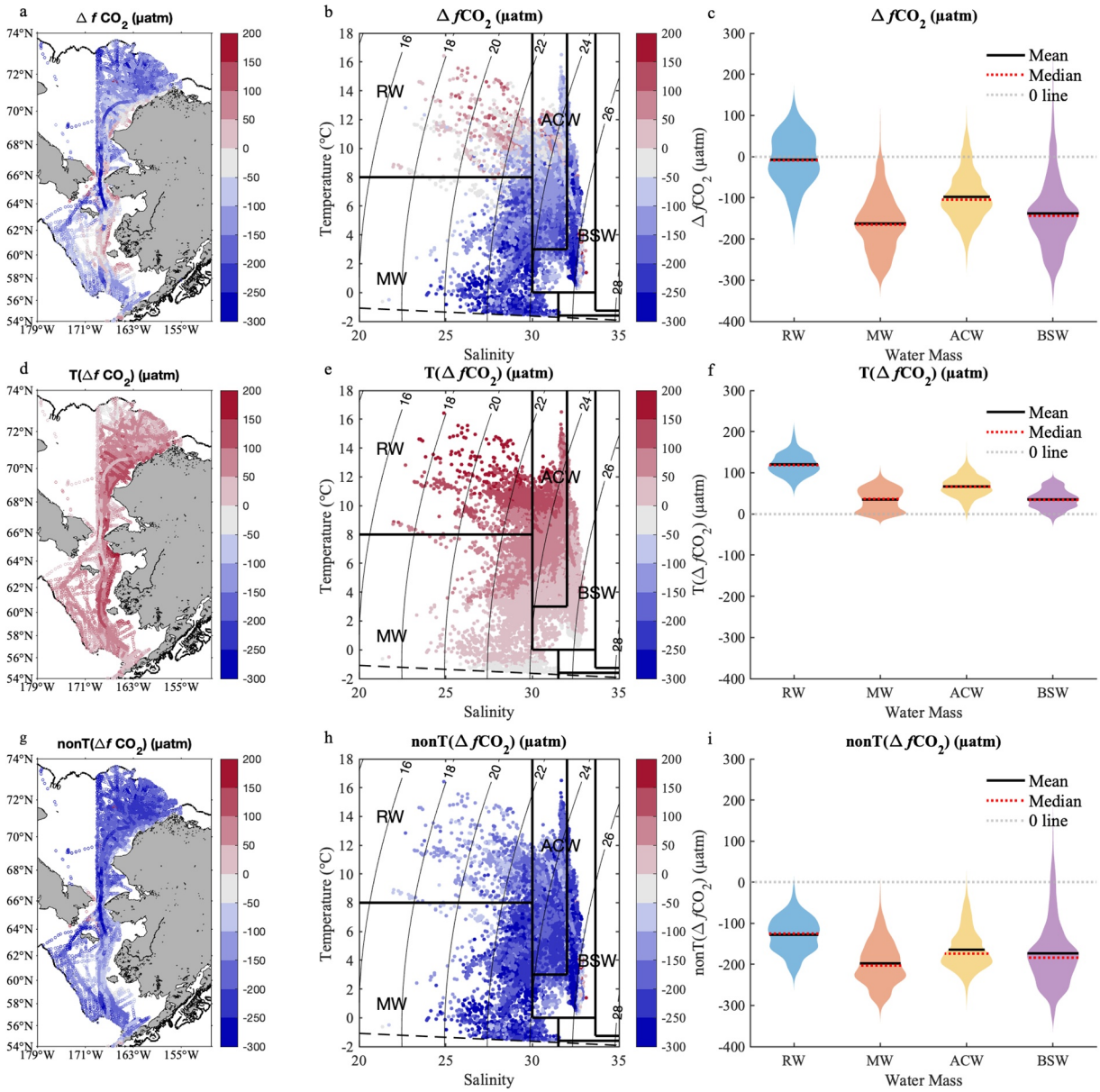

Figure 2. Water mass carbonate chemistry characteristics in the Bering and Chukchi Sea shelves, showing ΔfCO_2 (top row: a, b, c); $T(\Delta fCO_2)$ (middle row: d, e, f); and $\text{nonT}(\Delta fCO_2)$ (bottom row: g, h, i) by geographical distribution (left column: a, d, g); *T*/*S* characteristics (middle column: b, e, h) and via violin plots (right column: c, f, i). Note that the width of the violin curve corresponds with the kernel density of the data. Water mass designations follow Table 1, such that RW, River Water; MW, Meltwater; ACW, Alaskan Coastal Water; and BSW, Bering Summer Water. In the *T*/*S* diagrams, the dashed line is the freezing line.

Bering and Chukchi Sea shelves was −105 ± 77 μatm (mean ± standard deviation, $\Delta fCO_2 < 0$; cool colors, Figure 2a): the majority of the studied areas served as CO_2 sinks. There were two notable regional exceptions: weak CO_2 sources near the Yukon river plume and the coastal region northeast of Pt. Hope on the Chukchi shelf (see Figure 1 for place names). The temperature/salinity (*T*/*S*) diagram of the surface data clearly showed that these positive ΔfCO_2 signals were found in RW ($T > 8$°C, and $S < 30$, Figure 2b). Overall, however, the RW ΔfCO_2 ranged from −100 μatm to 100 μatm, with the mean value close to a neutral state (Figure 2c).

Recall that spatial variations in $T(\Delta fCO_2)$ indicate the impact of temperature change on fCO_2 relative to the climatological mean temperature, while $\text{nonT}(\Delta fCO_2)$ indicates the combined influences of primary productivity, respiration, and possible sea-ice melt related water masses mixing on fCO_2. Below, we will discuss the influence of temperature and non-temperature mechanisms on each of the four water masses given in this dataset. In all

cases, temperature weakly increased ΔfCO_2 values above 0, influencing the surface water toward CO_2 outgassing (Figure 2f); similarly, non-thermal mechanisms substantially decreased ΔfCO_2 below 0, influencing surface water toward CO_2 uptake (Figure 2i). Nuance emerges from the differences between the balance of these two factors within each water mass.

RW had the warmest sea surface temperature during the sampling period (10.4 ± 1.3°C) relative to the climatological mean temperature (1.7 ± 0.7°C), which led to the highest average $T(\Delta fCO_2)$ value (120 ± 26 µatm, Figure 2f), and high RW fCO_2 because $T(\Delta fCO_2)$ tends to be sensitive to the fCO_2 when the temperature anomaly is higher (Takahashi et al., 2002). The mean nonT(ΔfCO_2) was −128 µatm in the RW, the weakest among all water masses (Figure 2i). While the majority of this nonT influence is related to the influence of primary production, river-related mechanisms can moderate production-driven CO_2 drawdown. Local river runoff transports water with a naturally high content of fCO_2 and organic matter (e.g., Cross et al., 2013), which can lead to local outgassing. Also, the low ratio of total alkalinity to dissolved inorganic carbon (TA/DIC) in fresh water decreases the buffer capacity in the nearshore regions, which can lead to higher surface ocean fCO_2. In summary, RW-impacted areas were either CO_2 sources or CO_2 sinks depending on the competing forces of changing temperature, respiration of allochthonous organic carbon, primary productivity, and water chemistry changes.

In the summer season the MW temperature (3.0 ± 2.8°C) versus that of the climatological mean (−0.6 ± 0.7°C) did not substantially impact fCO_2 differences: the $T(\Delta fCO_2)$ only increases by 35 ± 27 µatm (Figures 2e and 2f). Nutrient-rich Pacific-origin waters pass through Bering Strait to support a brief but intense period of water-column primary production after the ice retreats. In our dataset, this process led MW to exhibit the strongest negative nonT(ΔfCO_2). Meanwhile, the seasonal cycle of sea ice also plays a role in regulating the inorganic carbon system. Melting of sea ice during the summer period results in a strong halocline with surface waters well below atmospheric CO_2 saturation, thus enhancing the uptake of atmospheric CO_2 into the ocean (Cross et al., 2013; Rysgaard et al., 2009). Together, these non-thermal processes decreased the ΔfCO_2 by an average of −198 ± 53 µatm (Figure 2i) in the dataset, which further confirms the importance of non-thermal CO_2 removal in MW. With the weakest $T(\Delta fCO_2)$ and strongest nonT(ΔfCO_2) influences, the ΔfCO_2 values in MW (average of −162 ± 68 µatm) were the most negative among all water masses (Figure 2c). Moreover, only 1% of the MW sampling points acted as a CO_2 source; thus, we can attribute a persistent seasonal CO_2 sink to this water mass.

The summertime average temperatures of ACW and BSW were 6.0 ± 2.0°C and 3.5 ± 2.3°C higher than their climatological means, respectively, reflecting an increase of 67 ± 26 µatm and 35 ± 23 µatm for their $T(\Delta fCO_2)$ (Figure 2f). The majority of the nonT(ΔfCO_2) values along the ACC were negative, suggesting a robust summer biological carbon removal. Interestingly, seasonal ΔfCO_2 and nonT(ΔfCO_2) were sporadically positive in the BSW (Figures 2a, 2b, 2g and 2h). These positive ΔfCO_2 points were generally found in the northern Chirikov Basin and along the central channel flow in the southeastern Chukchi Sea (Lin, Pickart, Moore, et al., 2019). The energetic flow (>25 cm s^{-1}, Woodgate et al., 2005) near Bering Strait induces strong lateral and vertical mixing, enhancing nutrient flux from bottom waters into the euphotic zone (Grebmeier et al., 2015). However, nutrient-enriched bottom water is also enriched in fCO_2, and vertical mixing also brings some of this CO_2 back to the surface (e.g., Creamean et al., 2019). In our dataset, the BSW water located in the Chirikov Basin and southern Chukchi Shelf had the highest monthly fCO_2 variability, ranging from 78 to 626 µatm (Figures 2b and 2c; discussed in more detail in Section 4.3.1).

4.2. Strong CO_2 Sinks

Negative ΔfCO_2 was present throughout most of the study area (Figure 2a). As such, here we constructed the geographical distribution of the large negative values (lower than the mean minus one standard deviation, i.e., <−182 µatm) to derive additional insights. Figure 2g indicates that all of the large negative values were associated with the nonT(ΔfCO_2) component. Geographically, they were located mainly in two regions (Figure 3a): in the general vicinity of Bering Strait (between 62°N and 70°N) and the northeastern Chukchi shelf around Hanna Shoal (north of 70°N), denoted by the dashed boxes in Figure 3a. We note that there is a paucity of data on the Russian part of the shelf; in that region, there may have been large negative values in the western pathway, which carries high-nutrient and low-fCO_2 Anadyr water (e.g., Creamean et al., 2019; Linders et al., 2017).

Plotting the large negative values in *T/S* space revealed that the northern cluster (near Hanna Shoal) largely fell within the category of MW (Figure 3b). This signal was present from July to September. Previous stud-

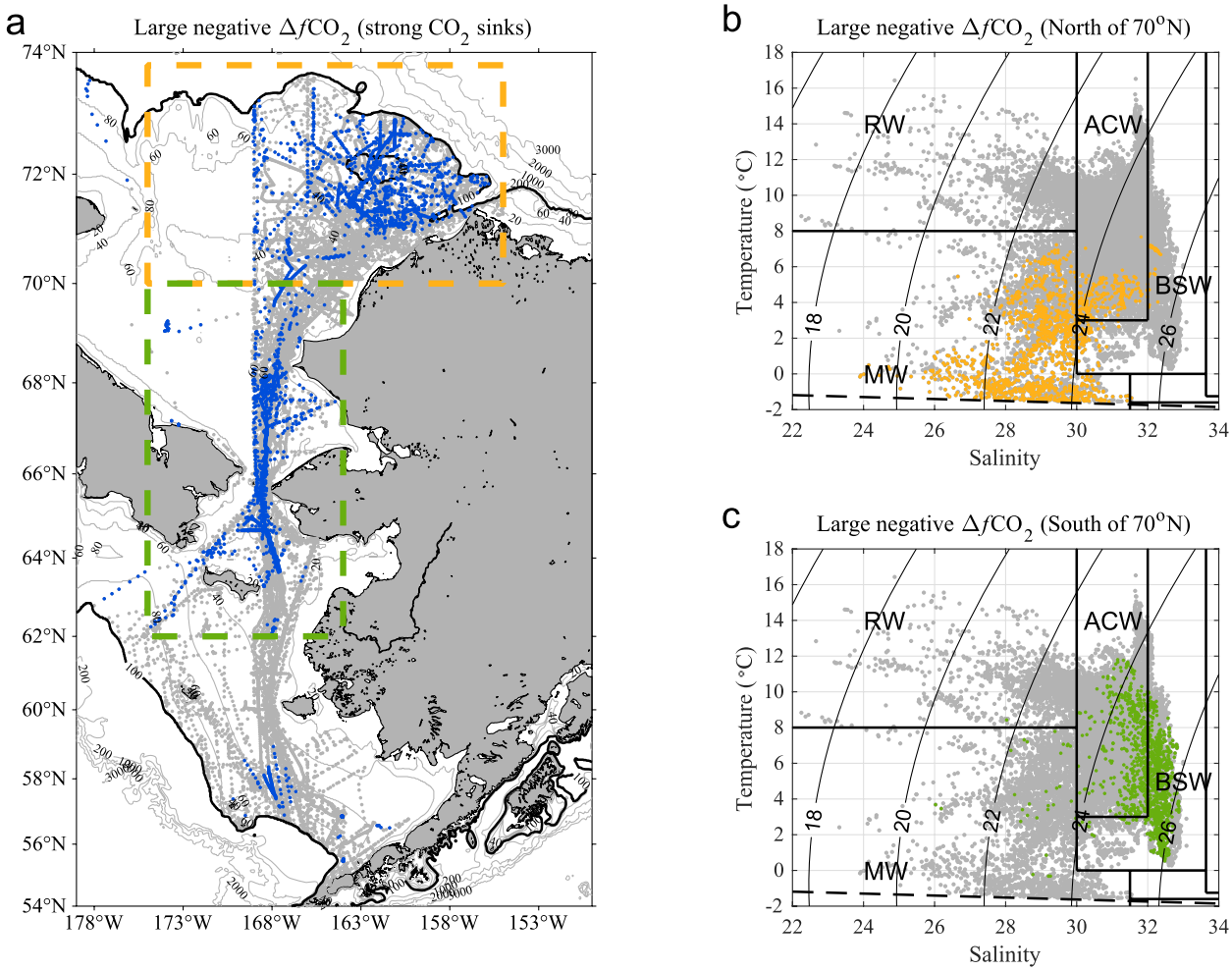

Figure 3. (a) Spatial distribution of large negative ΔfCO_2 (blue dots) in the northern and southern regions. The gray dots in all panels denote the remaining data throughout the full domain. The orange and green dashed boxes mark the northern and southern regions, respectively, shown in the *T/S* plot on the right. (b) The *T/S* values associated with large negative ΔfCO_2 north of 70°N (orange dots). (c) Same as (b) except for south of 70°N (green dots). In the *T/S* diagrams, the dashed line is the freezing line and water mass designations follow Table 1, such that RW, River Water; MW, Meltwater; ACW, Alaskan Coastal Water; and BSW, Bering Summer Water.

ies have shown that net community production near Hanna Shoal can reach up to 1.5 g C m^{-2} d^{-1} (Mathis et al., 2009). Juranek et al. (2019) and Ouyang et al., (2021) also found that significant biological activity drives a strong carbon sink in this area based on $\Delta O_2/Ar$ and ΔfCO_2 observations. In this dataset, the northeastern Chukchi shelf was a strong CO_2 sink during the open water season because of the high rates of primary production.

Most of the large negative ΔfCO_2 in the southern cluster was composed of BSW and ACW (Figure 3c). As noted above, the former is a mixture of water emanating from the Gulf of Anadyr and the central Bering shelf, while the latter results from runoff along the coast of Alaska. The primary productivity in this region occurs almost exclusively in June and July, enhanced by seasonal warming and high nutrient inputs from the Anadyr Water which contribute to the negative surface ΔfCO_2 value (Chen & Gao, 2007; Cross, Mathis, Frey, et al., 2014; Cross, Mathis, Lomas, et al., 2014). Additionally, a strong CO_2 sink was also found in the southeastern Bering Sea, where active physical processes such as intensive tidal mixing and eddies may help bring nutrients into the euphotic zone and contribute to sporadic biological bloom activity (e.g., Kelley et al., 1971).

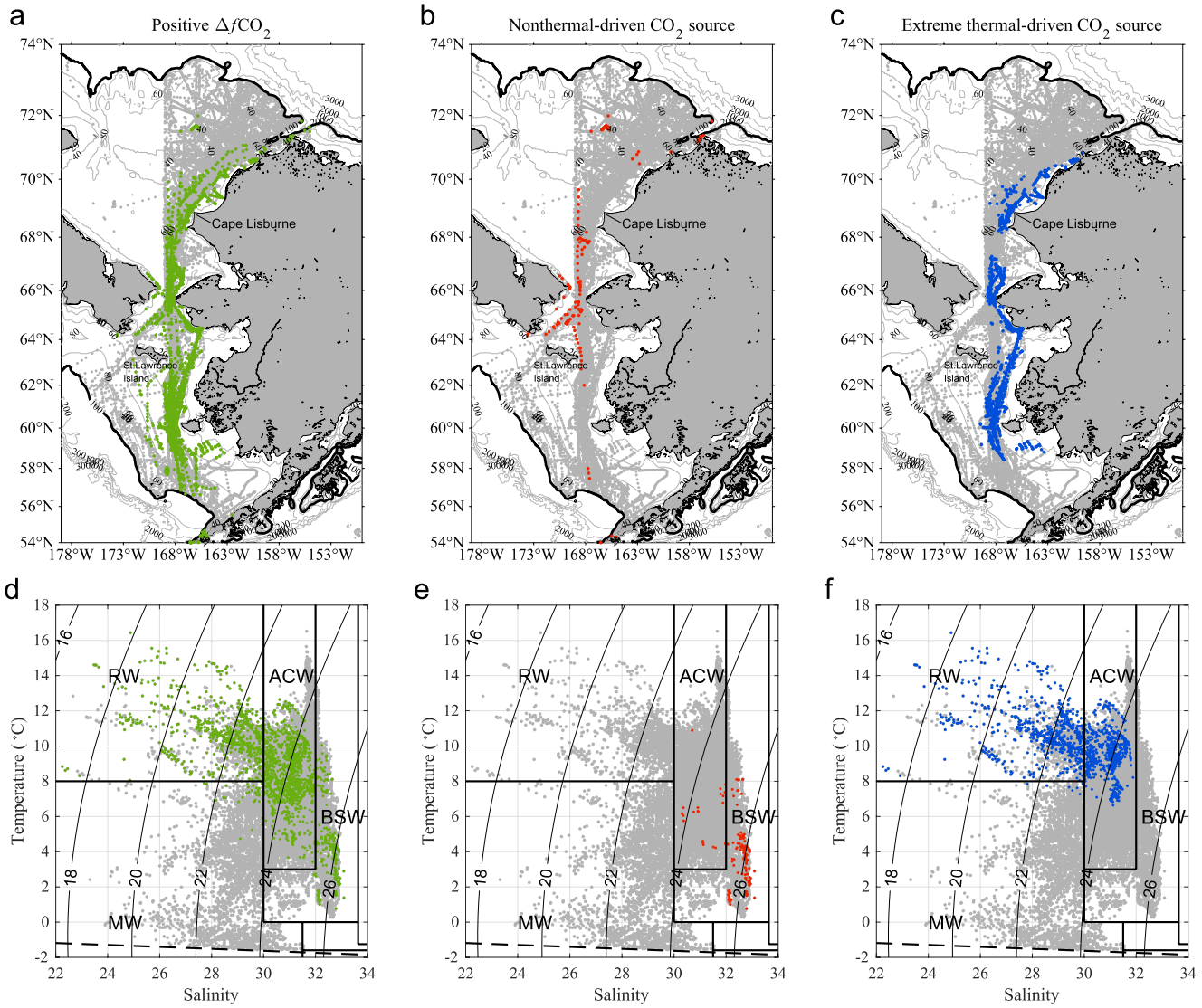

Figure 4. Positive ΔfCO_2 (green dots) by spatial distribution (a, b, c) and water mass (d, e, f). All positive values are highlighted at left (green dots, a, d); non-thermally driven data are shown in the center column (red dots, b, e); and extreme thermally driven data are shown at the right (blue dots; c, f). The gray dots denote the remaining data throughout the full domain. In the *T/S* diagrams, the dashed line is the freezing line and water mass designations follow Table 1, such that RW, River Water; MW, Meltwater; ACW, Alaskan Coastal Water; and BSW, Bering Summer Water.

4.3. CO_2 Sources

The locations of all the positive ΔfCO_2 values are shown in Figure 4a. South of Bering Strait, these were found along the Russian and Alaskan coasts, except for a Bering shelf water branch that bifurcates from the Alaskan coast toward the northwest and eventually mixes with Anadyr water (Sigler et al., 2017). North of the strait, positive ΔfCO_2 waters were found along the central channel and coastal pathways toward Barrow Canyon. The signal along the northern Siberian coast may reflect the Siberian Coastal Current (Weingartner et al., 1999). Associated with these pathways, the CO_2 sources were mainly provided by the ACW, BSW and RW (Figure 4d).

To address the dominant mechanism contributing to the CO_2 sources ($\Delta fCO_2 > 0$), we categorized CO_2 sources as either a non-thermally driven CO_2 source or extreme thermally driven CO_2 source. Figure 2 shows that nonT(ΔfCO_2) in the study area was -164 ± 63 µatm (Figure 2i), which means that net biological removal was the dominant process across the studied area during the warm season. As such, the relatively small number of instances when nonT(ΔfCO_2) is greater than $T(\Delta fCO_2)$ can be thought of as scenarios driven by non-thermal processes. By contrast, the $T(\Delta fCO_2)$ was 59 ± 34 µatm across the entire study area (Figure 2f). Hence, we chose

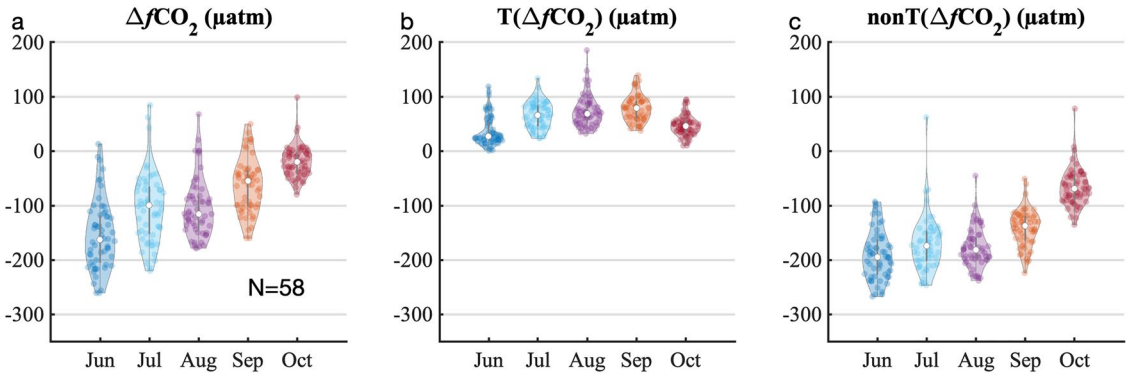

Figure 5. The distribution of (a) ΔfCO_2, (b)$T(\Delta fCO_2)$, (c) nonT(ΔfCO_2) in the 58 bins where all five summer months have data collected at resolution of 0.8° longitude × 0.4° latitude south of 70°N (or the green box in Figure 3).

$T(\Delta fCO_2)$ > 93 μatm (mean value plus one standard deviation, which is higher than the nonT[ΔfCO_2]) as the threshold for extreme cases of thermally driven CO_2 sources.

4.3.1. Non-Thermally Driven CO_2 Sources

Figure 4b shows that the CO_2 sources driven by non-thermal processes, mainly biological respiration, were generally located between St. Lawrence Island (~63°N) and Cape Lisburne (~69°N). North of Bering Strait this signal was found along the central shelf pathway, where the large negative ΔfCO_2 was present as well, although the latter was also found in the coastal pathway (compare Figures 4b and Figure 3a). BSW contributed most of the non-thermally driven CO_2 sources, with the remainder found in ACW (Figure 4e).

Recall that the strong CO_2 sink (non-thermally driven) also extends to the southern Chukchi Sea and northern Bering Sea, associated with ACW and BSW (Figures 3a and 3c). It is interesting to address the discrepancy between the non-thermally driven CO_2 source and strong non-thermally driven CO_2 sink. To do that with minimum sampling bias, we examined seasonality in the bins where all five summer months were collected at a resolution of 0.8° longitude × 0.4° latitude. There were in total 58 grids that fit our selection criteria south of 70°N. As Figure 5 shows, both ΔfCO_2 and nonT (ΔfCO_2) in later months was significantly higher than that in the early months, while $T(\Delta fCO_2)$ was lowest in October. The seasonality of ΔfCO_2 and nonT(ΔfCO_2) confirmed that the strong non-thermally driven CO_2 sink was more prevalent early in the season. In contrast, the non-thermally driven CO_2 source was the greatest in October, reflecting the seasonal variability in the biological pump. The abundance of nutrients advected by Anadyr water and the warming in early summer together enhance surface primary productivity and lead to a strong CO_2 sink (Cross et al., 2018). The rate of phytoplankton production then decreases over time and ultimately the organic carbon produced sinks to the bottom, where bacterial respiration returns CO_2 back to the water column late in the season (Cross, Thomas, Frey, et al., 2014; Cross et al., 2018).

Notably, during the period of non-thermally driven CO_2 source (nonT[ΔfCO_2] > T[ΔfCO_2]) in the Bering and Chukchi Sea shelves (Figure 4b), the mean wind was strong out of the north (wind speed >5 m s^{-1}, Figure 6a), which reduces the poleward flow (Woodgate et al., 2005). This decrease in velocity favors vertical organic carbon deposition and respiration. If the northerly wind lasts long enough, it can be conducive to wind-driven overturning, bringing respiration products to the surface (Creamean et al., 2019). In summary, the later season's positive ΔfCO_2 values mainly resulted from the release of respiration products from the early season's productivity.

4.3.2. Extreme Thermally Driven CO_2 Sources

Extreme thermally driven CO_2 sources (T[ΔfCO_2] > 93 μatm) were generally found along the pathway of the ACC, associated with very warm ACW and RW (Figures 4c and 4f). Mean winds when $T(\Delta fCO_2)$ > 93 μatm were very weak over the northern Bering and Chukchi Sea shelves (wind speed <1 m s^{-1}, Figure 6b). Accordingly, wind-driven mixing was negligible, allowing surface waters to heat more readily. This heat contributed to increases in ΔfCO_2 to the point of equilibration and outgassing, leading to the development of temperature-driven CO_2 sources (Figures 2e and 2f). It should also be noted that weak wind mixing limits the nutrient supply from depth necessary for rapid and intense primary production, meaning that there is little competition with temperature controls on ΔfCO_2. The signal of extreme thermal-driven CO_2 sources, carried northward by the ACC, disappears at

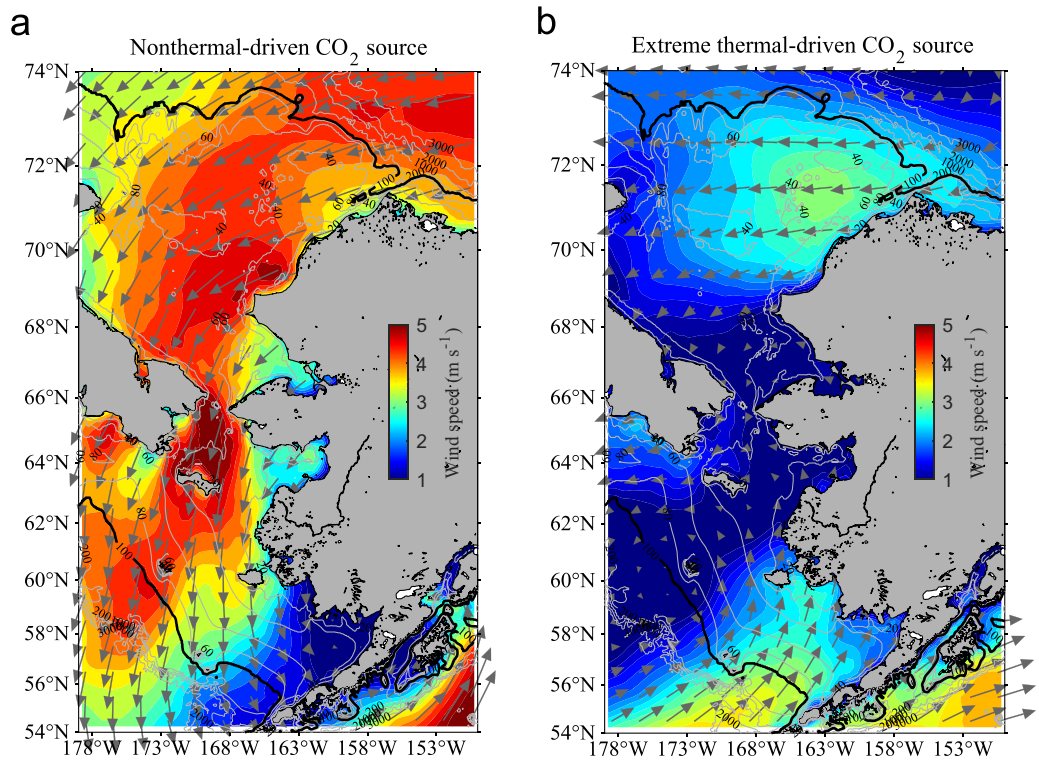

Figure 6. Mean wind speed (color) overlain by the 10 m wind vectors when (a) the non-thermally driven CO_2 source (nonT[ΔfCO_2] > T[ΔfCO_2]) and (b) the extreme thermally driven CO_2 source ($T(\Delta fCO_2)$ > 93 μatm) occurs. The northerly wind favors offshore Ekman export and upwelling in nearshore areas, while the southerly wind favors the heat transport into the Chukchi Sea.

the head of Barrow Canyon. Recall that the Central Channel pathways eventually merge with the coastal current in the vicinity of the canyon (Lin, Pickart, McRaven, et al., 2019; Lin, Pickart, Moore, et al., 2019). The strongly negative ΔfCO_2 water stemming from the region of Hanna Shoal (Figure 3a) thus offset the positive ΔfCO_2 in the coastal current where the different water masses join together and mix.

5. Long-Term Change of ΔfCO_2

5.1. Sea-Air CO_2 Difference Changes

The time series of surface ΔfCO_2 considered here provides us with the opportunity to investigate long-term changes in carbon sinks and sources in these highly variable coastal regions, which in turn sheds light on the changing contributions of the processes affecting the ocean carbon chemistry. The fundamental question is: how is ongoing Arctic environmental change impacting the regional carbon cycle?

The first step in an analysis of this type is to investigate any change between two time bins. In unevenly distributed datasets like these, the cutoff between bins can impact the results (Fay & McKinley, 2013); accordingly, to determine the sensitivity of the choice of the year, we computed the ΔfCO_2 difference with different dividing years (Figure S3 in Supporting Information S1). Even though the absolute values slightly differ with different start and end date selection, the main spatial patterns are the same. To facilitate the following discussion, we used the mean summer ΔfCO_2 changes between post-2014 (2014–2019) and pre-2014 (1989–2013) as an example to show the long-term changes of ΔfCO_2. Figure 7 shows the total magnitude of the ΔfCO_2 change between the two time periods: ΔfCO_2 in the northern Chukchi Sea increases in recent years compared to the early record (warm colors, Figure 7c); Meanwhile, ΔfCO_2 mostly decreases north of St. Lawrence Island and in the southeast Bering Sea (cold colors, Figure 7c).

To detect a significant CO_2 change, the external signal must equal or exceed twice the internal noise (Carter et al., 2019). The internal noise of fCO_2 mainly consists of the measurement uncertainty (±2 μatm), short-term

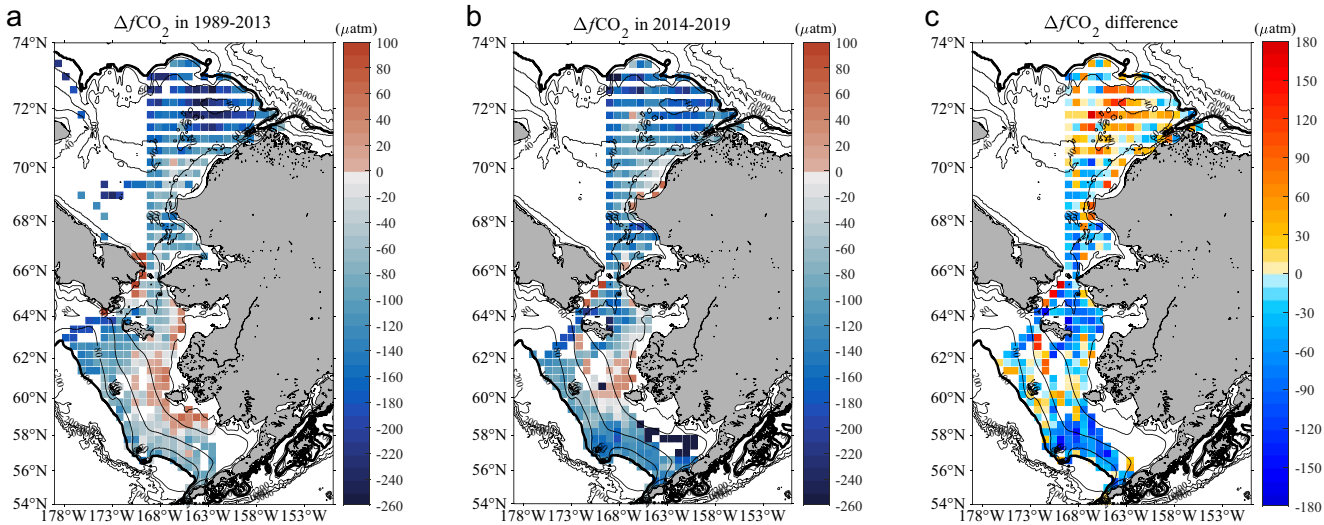

Figure 7. Gridded means surface ΔfCO_2 at 0.8° (longitude) × 0.4° (latitude) in the periods of (a) 1989–2013, (b) 2014–2019, and (c) the difference between these two periods.

(daily, seasonal), interannual and decadal natural variability. Given that we compared the mean state of summer-only data, the short-term variability has been averaged out and can be neglected. Therefore, the major contributors of the internal noise in this study are the interannual and decadal natural variability, caused by the large-scale climate patterns such as the Pacific Decadal Oscillation and El Nino/Southern Oscillation.

It is challenging to evaluate decadal and multidecadal natural variability in carbon system parameters fully, especially in areas with limited time series data such as the Alaskan shelf and Arctic Ocean. Based on 81 sets of measurements in 21 years, Carter et al. (2019) reported 27 μatm total natural variability calculated from a deseasonalized fCO_2 dataset near Unimak Pass in the Alaskan Aleutian Islands. This site has the best temporal resolution of fCO_2 data in all of coastal Alaska, owing to the high amount of vessel traffic through this pass. While this reference point is near the southern boundary of the data used in this study and ideally would not be applied across our entire, highly variable study area, it represents the closest metric we have to understanding decadal fluctuations. Further, the dataset we have assembled here does not have the temporal resolution of the Carter et al. (2019) study (although we do have the advantage of a much greater spatial resolution), and calculating such values from our dataset would introduce insurmountable sampling bias. Accordingly, we adopted the 27 μatm value from Carter et al. (2019) to represent the envelope of natural variability across this study. Therefore, if the fCO_2 difference between any two periods falls in the range of $\pm 27 \times 2 = \pm 54$ μatm, the calculated temporal change only reflects the natural variability. Otherwise, the long-term change has emerged from the envelope of natural variability.

The sea-air CO_2 flux equates to CO_2 solubility × gas exchange coefficient × ΔfCO_2 (Wanninkhof, 2014). Among the different elements, ΔfCO_2 sets the direction of CO_2 flux and potential of CO_2 flux, while the gas exchange coefficient exponentially increases with the wind speed. ERA5 provides a robust wind product that has a good correlation with the observations, and has been used in many previous studies (e.g., Lin et al., 2020; Tian et al., 2021).

To avoid the complexity caused by snapshots of highly variable wind speed, we first calculated the mean summer (June to October) wind speed in the periods of 1989–2013 (Figure S4a in Supporting Information S1) and 2014–2019 (Figure S4b in Supporting Information S1). It reveals that the change of the mean wind speed in these two periods is minor on the Bering Sea shelf (0.98 m s^{-1} vs. 0.91 m s^{-1}), as well as on the Chukchi Sea shelf (1.6 m s^{-1} vs. 1.9 m s^{-1}). Then, after multiplying by the mean sea-air CO_2 differences in each period (Figures 7a and 7b), we determined the average sea-air CO_2 flux in 1989–2013 and 2014–2019, and ultimately their flux changes. With the regional mean summer wind speed, SSS and SST, a fluctuation of ±54 μatm fCO_2 would lead to the uncertainties of ±0.1 mmol C m^{-2} d^{-1} and ±0.3 mmol C m^{-2} d^{-1} sea-air CO_2 flux on the Bering and Chukchi sea shelves, respectively. Similar to the fCO_2 variability, any flux change between two periods less than ±0.1 mmol

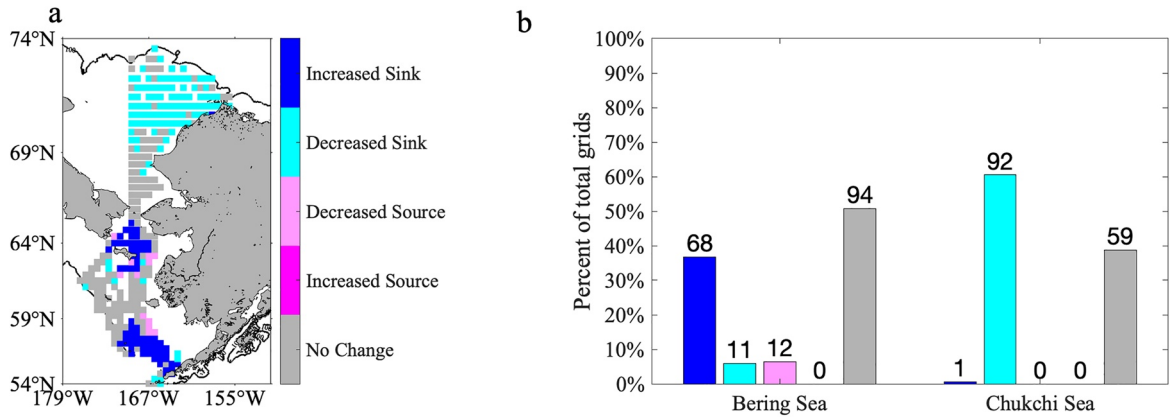

Figure 8. Statistical changes in CO_2 sinks and sources between pre-2014 and post-2014 in the Bering and Chukchi Sea shelves, by (a) Spatial distribution and (b) the *n* and percentage of data falling within each category. The bin size in (a) is the same as that in Figure 7c. Note, the natural variability of sea-air CO_2 flux change on the Bering and Chukchi Sea shelves was ±0.1 mmol C m^{-2} d^{-1} and 0.3 mmol C m^{-2} d^{-1}. The flux uncertainty was calculated based on SSS = 31.3, SST = 8.2°C, wind speed = 0.9 m s^{-1}, and SSS = 30.2, SST = 4.4°C, wind speed = 1.7 m s^{-1} in the Bering and Chukchi Sea shelves, respectively.

C m^{-2} d^{-1} on the Bering Sea shelf, or ±0.3 mmol C m^{-2} d^{-1} in Chukchi Sea shelf is taken to reflect the natural variability. Figures 8a and 8b show the regional breakdown of changes in CO_2 sources and sinks.

The carbon flux in 51% (n = 94) of the bins on the Bering Sea shelf did not significantly change, especially near the Yukon River plume. Hence, the CO_2 flux change, that is, decreasing CO_2 sink or source, near the Yukon River outflow mainly reflects the natural variability (it is possible that natural variability near the Yukon River plume may be greater than ±27 µatm). However, the CO_2 sink in the remaining 36% of bins (n = 68), either in the regions north of St. Lawrence Island or the south of 59°N got stronger between the two time periods. The large fraction of "no change" and stronger carbon sink bins is consistent with the earlier study of Takahashi et al., (2009), who found the Bering Sea oceanic CO_2 insignificantly decreased at rate of −1.2 ± 1.2 µatm yr^{-1} from 1974 to 2004. Additionally, Takahashi et al. (2014) shows, using climatological data between 2000 and 2005, that Bering Sea surface oceanic CO_2 decreased in August but increased in February, which further agrees with our conclusion that this fCO_2 change mainly reflects natural variability rather than long term changes.

In contrast to the Bering Sea shelf, only 39% of bins (n = 59) show insignificant change in the Chukchi Sea, reflecting only natural variability. The CO_2 sinks in only one bin in the Chukchi Sea shelf strengthened in recent years, while 61% (n = 92) weakened (Figure 8b), making the majority Chukchi Sea shelf a weaker carbon sink after 2014 (Figure 8a). These findings are different from an earlier report by Ouyang et al., (2020), who found a stable mean surface CO_2 across the Chukchi Sea shelf based on sea-air CO_2 difference only. We think differences in the data treatment can partially explain these different results, because averaging the entire Chukchi Sea CO_2 records in Ouyang et al. (2020) have smoothed out the spatial variability as we found in this study (Figure 7c).

The above results (Sections 4.1 and 4.2) have shown that the spring bloom occurs earlier in the Bering Sea than in the Chukchi Sea. It is interesting to see a weakening Chukchi Sea shelf sink during peak production times, but a strengthening Bering Sea shelf sink outside of the typical primary production season. What might be the cause of these counterintuitive, opposing trends?

5.2. Mechanisms Driving Long-Term Changes in Sea-Air CO_2 Differences

To shed further light on the underlying mechanisms controlling this long-term variability, we again use a temperature normalization analysis to distinguish non-thermally driven long-term changes from thermally driven long-term changes (Figure S5 in Supporting Information S1). The non-thermally driven change is assigned when changes in the absolute nonT(ΔfCO_2) changes between post-2014 and prior-2014 are higher than that of T(Δf-CO_2). Otherwise, it will be attributed to thermally driven change. The long-term changes of sea-air CO_2 differences over the vast majority of the study areas were due to non-thermal, or biological processes (Figure 9a). However, there was a signature of thermally driven changes along the coastal pathway in the northern Bering Sea

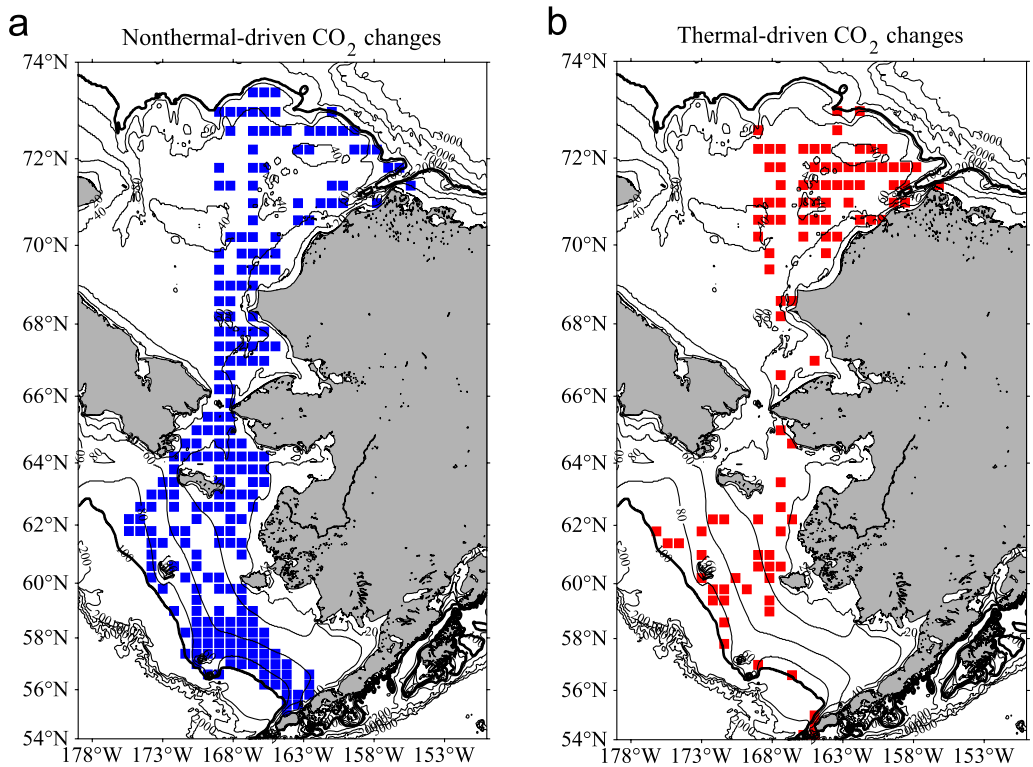

Figure 9. Locations where the long-term change in ΔfCO_2 from 1989–2013 to 2014–2019 was dominated by (a) non-thermal and (b) thermal processes.

and Chukchi Sea shelves (Figure 9b). The same was true of the region on the Chukchi shelf south of Hanna Shoal and in the middle part of the Bering Sea shelf.

Over the time period in question, a notable decline in sea-ice concentration occurred (e.g., Duffy-Anderson et al., 2019; Frey et al., 2015), where ice losses in the Chukchi Sea have outpaced much of the Arctic (Arthun et al., 2021). The associated shifts in heat and salt fluxes have been so large they have changed the hydrographic structure in the interior basin (e.g., Timmermans et al., 2018). Figure 10 shows that, compared to the earlier period, the duration of ice cover significantly decreased in the recent six years on the northeastern Chukchi shelf

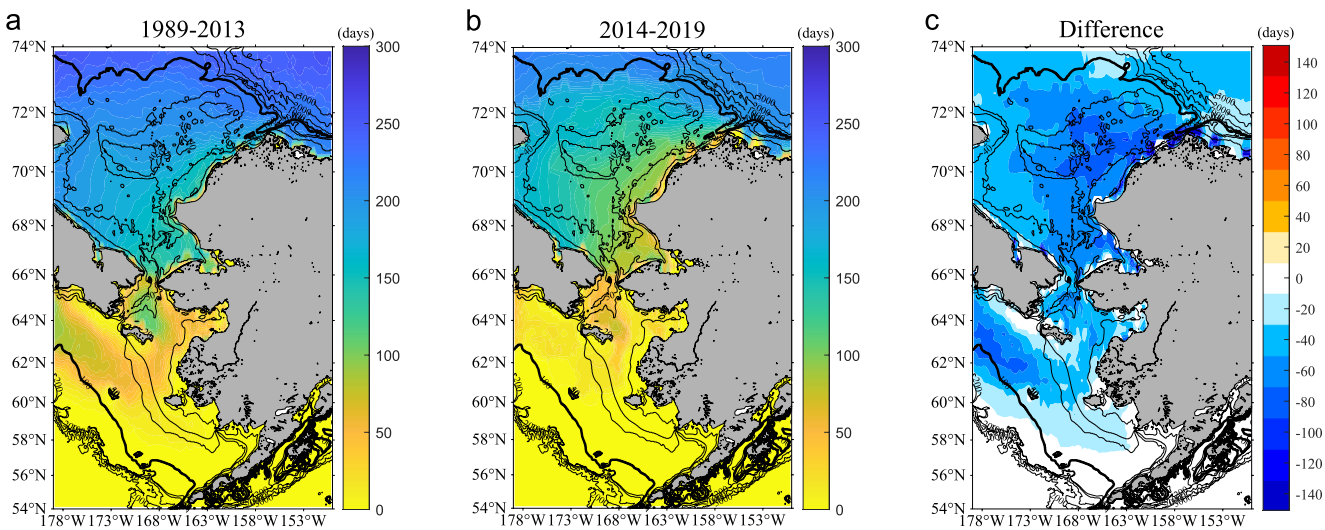

Figure 10. Mean annual duration of ice cover in the periods of (a) 1989–2013, (b) 2014–2019, and (c) the difference between the two periods.

and on the Bering shelf in the vicinity of Siberia. This is consistent with Danielson et al. (2020) who reported unprecedented low winter and spring sea-ice cover from 2014–2018 in the northern Bering and Chukchi Seas. As we have demonstrated earlier with our dataset (see Figure 4 and accompanying text), sea ice melt caused the surface mixed layer to shallow and warm more quickly, while phytoplankton productivity slowed due to nutrient limitation. Is this the same mechanism driving the long-term temporal ΔfCO_2 variability seen here?

Based on the known relationship between temperature and oceanic fCO_2 (Takahashi et al., 2002), we can compute the average oceanic fCO_2 changes caused by direct warming over time on the northern Chukchi shelf (70–74°N). The recent warming from an average temperature of 1.9°C–5.4°C between 1989–2013 and 2014–2019 on the Chukchi Sea shelf (Figure S6 in Supporting Information S1) can increase the mean surface fCO_2 from 234 µatm to 272 µatm ($234 \times \exp[0.0423 \times 3.5]$). This predicted value is only 2 µatm higher than the mean observed fCO_2 value (270 µatm) during 2014–2019. Therefore, the warming associated with the intensified sea-ice loss can explain the majority ΔfCO_2 increase in the northern Chukchi Sea.

The minor impact of non-thermal processes in Chukchi Sea may reflect the high interannual variability of primary productivity, meaning that external change of primary productivity has not emerged from background internal variability. A recent study by Woodgate and Peralta-Ferriz (2021) reported that the Pacific flow across the Bering Strait has warmed and freshened from 1990–2019, especially after the year 2014. They hypothesized that the dramatic property change may impact the nutrient ventilation in the Chukchi Sea. This has been borne out in other studies: Stabeno et al. (2019) pointed out that a decrease in nutrient content near M8 mooring site in the northern Bering Sea was associated with freshening of Pacific Winter Water. Mordy et al. (2020) showed that the pre-bloom nutrient concentrations in the Chukchi Sea directly correspond to the fall nutrient concentrations at M8 mooring (62.194°N, 174.688°W, northern Bering Sea), and that the dissolved inorganic nitrogen concentration in M8 bottom water declined by ~37% between 2005 to 2016 (Mordy et al., 2020). This nutrient decrease may reflect a summer nutrient limitation in the Chukchi Sea. Meanwhile, Lewis et al., (2020) suggested that increased Pacific Summer Water brings more nutrients onto the Chukchi shelf, which supports a higher primary production. They also found a significant increase in primary productivity on the Chukchi Sea over time. These "contradicted" studies actually reveal the highly variable dynamic of primary productivity. Even though the long-term changes of primary productivity are still unclear in the Chukchi Sea because of high year-to-year variability, the dominant role of thermal processes in long-term changes in northern Chukchi Sea CO_2 sink offers a potential glimpse of the broader CO_2 sink changes under future warming projections.

Of additional interest is the rate of average summer fCO_2 increase over time in northern Chukchi Sea surface waters (70°N–74°N). We use the average increase from 234 µatm to 272 µatm to estimate the long-term changes. Using the middle sample year in each period (2008 and 2018, respectively), this gives an annual rate of 38 µatm fCO_2/10 years, or 3.8 µatm fCO_2 yr^{-1}. Even though this average rate is higher than that in the open ocean regions (1.5–2 µatm yr^{-1}) (Sutton et al., 2019; Takahashi et al., 2009), the trend uncertainty (±9.7 µatm) caused by the spatial variability prevents us from comparing with the rates robustly in the open ocean. Others have found that the volume of undersaturated, acidified water in the Pacific halocline downstream from the Chukchi shelf is growing over time (Qi et al., 2017). If surface ocean fCO_2 continues to increase over time, this could mark the Chukchi Sea as a seasonal ocean acidification hotspot.

On the Bering Sea shelf, the mean fCO_2 prior to 2014 was 328 µatm. Using the same temperature normalization technique, we found that the warming on the Bering Sea shelf would increase this value to 349 µatm fCO_2, based on the increase in sea surface temperature from 7.5°C to 9.0°C between the two periods. However, the observed mean fCO_2 in the latter period was 303 µatm, which translates to an annual decrease in CO_2 of −1.6 µatm yr^{-1} over a 10-year period. Unlike in the Chukchi Sea shelf, we speculate that enhanced primary productivity on the Bering Sea shelf can overcome the impact of warming, even though warming and increased meltwater can increase the stratification and reduce the nutrient flux from depth. The weakened CO_2 source near the Yukon River outflow also shows this area becomes less heterotrophic over time, also overbalanced by strong autotrophic processes.

The year-to-year variation of biological activity on the Bering Sea shelf makes the estimation of long-term changes of primary productivity difficult based on direct observation. Some studies indicate that primary production would have to change by 60% before a long-term trend could be detected (Lomas et al., 2012; Mordy et al., 2012). In part, this large inter-annual variability is linked to oscillating climatic states: integrated net

primary productivity increased from colder periods (e.g., 2007–2012) to warmer periods (e.g., 2014–2018) because of almost twice as high growth rates in the warm years (Lomas et al., 2020). Particulate organic carbon fluxes in Bering shelf waters were in the range 0.8–2.3 g C m^{-2} d^{-1} in 2018, which also confirms the extraordinary strength of the biological carbon pump during warm years (O'Daly et al., 2020). Consequently, it would be difficult to identify a multi-decadal trend in primary productivity in the Bering Sea. The CO_2 sink may continue to increase on the northern Bering shelf because nutrients are unlikely to become limited there, due to the consistent influx of nutrient-rich Anadyr Water via the Anadyr Current (O'Daly et al., 2020). Assuming the lateral export is stable over time, we could expect that bottom water in the Bering Sea may experience a much higher absorption of anthropogenic CO_2 – and consequently more intense acidification events–because more freshly produced organic carbon may sink and get respired in bottom waters, leading to the intermittently reported bottom calcium carbonate undersaturation states and a bottom water ocean acidification hotpot (Cross et al., 2013; Mathis et al., 2011a, b, 2014). However, the sparsity of water column data limits our ability to quantify the carbonate system in deep water. Future study needs to fill this data gap, for example, using moored water samplers at depth (e.g., Mathis et al., 2014).

It is important to note that the long-term ΔfCO_2 variation documented here is not analogous to the anthropogenic CO_2 trend. First, our analysis is based on a single season of data, not data collected across the entire year. As technology advances and scientists collect more data during different seasons, it will be helpful to understand the annual ΔfCO_2 changes. Second, the observed CO_2 includes the impacts of all short-lived thermal and non-thermal processes, but may not fully represent the average seasonal conditions because extreme events can heavily modify the observed values. This phenomenon may not be uncommon since fCO_2 data were only collected sporadically before 2017 in these vast, dynamic systems. Third, the CO_2 spatial and temporal changes reported in this study could be biased by the increased sampling in the month of August versus the other summer months in deriving the long-term averages (Figure S1 in Supporting Information S1). Therefore, we need to be cautious in interpreting the long-term variability. That said, the time series to date can still provide a glimpse of the summer oceanic CO_2 changes under global warming. In the coming decades, autonomous research vehicles, float sensors, and profiling floats will tremendously enrich the data coverage, which has strong potential to reduce the uncertainty of long-term changes.

5.3. Open Questions Related to Sea Surface Salinity Changes

Accompanying the rapid sea-ice loss in the northern Chukchi Sea, the sea surface salinity increased 3–4 from pre-2014 to post-2014 (Figure S6 in Supporting Information S1), which is counterintuitive in light of the overall Arctic Ocean freshening (Brown et al., 2020; Woosley & Millero, 2020). However, this positive salinity anomaly is also reported by Danielson et al. (2020) based on an independent hydrographic dataset from the 1920s–2010s. Therefore, the positive salinity anomaly is emerging as a new phenomenon in recent years, and could have implications for the carbon system.

There are a few processes that can contribute to salinity changes. First, sea-ice does not melt with spatial consistency in the Chukchi Sea. The thinner ice pack in recent years can easily be broken-up and exported off the Chukchi shelf by a combination of the wind and currents before melting remotely. Because current- and wind-driven export of the ice pack can cause melt signals to move spatially, a freshwater deficit could be caused by local formation but non-local melt of Chukchi sea ice (Danielson et al., 2020).

Second, the August northerly wind speed intensified over the Chukchi and northern Bering Sea shelves in recent years compared to the start of the dataset (Figure 11). Strong winds in any direction could deepen the mixed layer, causing a typical summer melt signal to be diluted over a larger volume, and thereby increasing salinity over time. However, a strong northerly wind results in enhanced offshore Ekman export that could overturn underlying high salinity and fCO_2 BSW or Winter Water to the surface layer. Past studies show that sustained high winds (>10 m s^{-1}) can induce vertical mixing that provides nutrients for phytoplankton productivity and ephemeral, wind-driven CO_2 effluxes above (e.g., Crawford et al., 2020; Creamean et al., 2019). Accordingly, the disturbed or uplifted pycnocline can lead to positive salinity anomalies in the newly ice-free waters. This could also help explain the faster-than-average growth in surface seawater fCO_2 in the Chukchi Sea over time. The precise reasons for the positive salinity anomaly are beyond the scope of this study; future study is required to unravel the mechanisms and their implications for the changing carbon cycle in the Chukchi Sea.

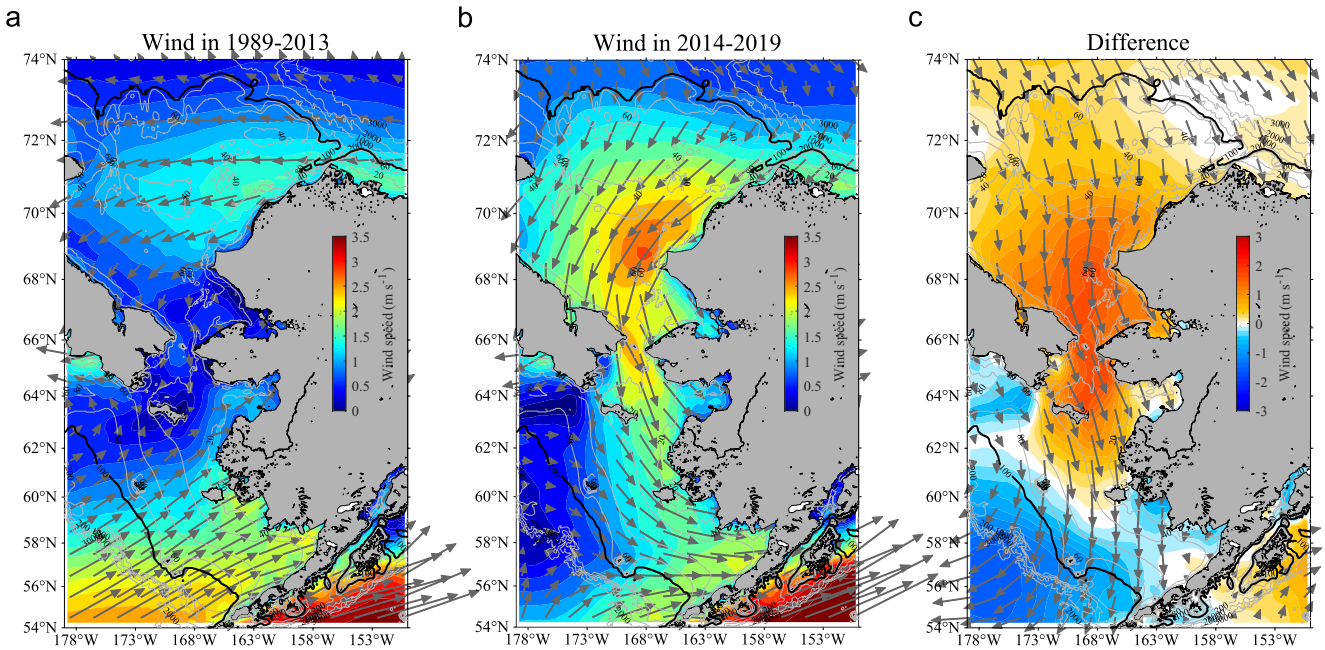

Figure 11. Mean August wind speed (color) overlain by the 10 m-wind vectors in the periods of (a) 1989–2013, and (b) 2014–2019. (c) The difference between the two periods.

6. Summary

Our synthesis of summertime surface underway CO_2 measurements from 1989 to 2019 has provided a unique opportunity to study the spatial and temporal variability of the sea-air CO_2 differences (oceanic fCO_2 minus atmospheric fCO_2, ΔfCO_2) on the Bering and Chukchi Sea shelves. It was demonstrated that primary productivity is the dominant mechanism maintaining the strong summer CO_2 sink in the region. In early summer, Bering Summer Water provides the nutrients to sustain the high net primary productivity in the northern Bering Sea, and on the Chukchi shelf within the central channel flow and near Hanna Shoal. However, later in the season, northerly winds induced strong upwelling and vertical mixing near Bering Strait and in the central channel flow. This releases the early season's respiration products back to the surface, resulting in CO_2 outgassing. Moreover, rapid seasonal warming, and respiration of labile organic carbon in river runoff, make the nearshore areas a weak seasonal carbon source.

The long-term response of the seasonal carbon cycle to climate change on the Bering and Chukchi Sea shelves was also investigated. Our data synthesis shows that global warming, sea-ice loss, and biological activity all synergistically impacted the summertime carbon cycle between the pre-2014 and post-2014 periods. On the Chukchi Sea shelf, rapid warming following sea ice melt led to a moderately high growth rate in summer surface ocean CO_2 over time. By contrast, enhanced primary productivity on the Bering Sea shelf augmented the carbon sink and slowed the growth of summer surface ocean CO_2 over time. While more data will be necessary to explore year-round expressions of the carbon cycle, including rates of ocean acidification, overall this dataset has illustrated heterogeneous feedbacks to climate change in sub-Arctic seas and offers a snapshot of the broader carbon cycle changes under future warming and low-ice projections.

Data Availability Statement

The SOCAT data can be downloaded from https://www.socat.info/index.php/data-access/. The CO_2 collected by saildrone unmanned surface vehicles in summer of 2017, 2018 and 2019 are publicly available through NOAA's National Centers for Environmental Information NCEI (with DOIs: https://doi.org/10.25921/w59k-4b77, https://doi.org/10.25921/gkr5-cb26, https://doi.org/10.25921/kaj6-vc23, https://doi.org/10.25921/wkrh-a319, https://doi.org/10.25921/fdbj-6k06, https://doi.org/10.25921/tpv6-sk21).

Acknowledgments
The Surface Ocean CO_2 Atlas (SOCAT) is an international effort, endorsed by the International Ocean Carbon Coordination Project (IOCCP), the Surface Ocean Lower Atmosphere Study (SOLAS) and the Integrated Marine Biosphere Research (IMBeR) program, providing a uniformly quality-controlled surface ocean CO_2 database. The many researchers and funding agencies responsible for the collection of data and quality control are thanked for their contributions to SOCAT. We gratefully acknowledge the support of the funding agencies that supported this analysis, including the New Sustained Observations for Arctic Research project and the DBO-NCIS project (NA14OAR4320158, NA19OAR4320074) from the NOAA Arctic Research Program. Additionally, we are extremely grateful for the opportunity to use new saildrone measurements in this synthesis analysis, which would not have been possible without diligent support from Heather Tabisola, Calvin Mordy, and Christian Meinig from the Innovative Technology for Arctic Research Program at the NOAA Pacific Marine Environmental Laboratory, and QA/QC from Stacey Maenner, Sylvia Musielewicz, and Adrienne Sutton of the PMEL Carbon Group, and Natalie Monacci from the University of Alaska, Fairbanks Ocean Acidification Research Center. We also owe a debt of gratitude for this analysis to the officers and crew of USCGC *Healy*, from which many of the underway datasets were collected, and to the late Taro Takahashi and the Carbon Dioxide Research Group at Lamont Doherty Earth Observatory at Columbia University for support of this underway data collection for many years. Stimulating conversations about the interpretation of this dataset were also provided by our colleagues at the UW Cooperative Institute for Climate, Ocean, and Ecosystem Science and the PMEL Carbon and Eco-FOCI Groups. No science is possible without the support of our families, and the authors also thank their spouses and children for their continual career support. This manuscript is PMEL contribution number 5232.

References

Anderson, L. G., Falck, E., Jones, E. P., Jutterström, S., & Swift, J. H. (2004). Enhanced uptake of atmospheric CO_2 during freezing of seawater: A field study in Storfjorden, Svalbard. *Journal of Geophysical Research*, *109*, C06004. https://doi.org/10.1029/2003JC002120

Arrigo, K. R., van Dijken, G., & Pabi, S. (2008). Impact of a shrinking Arctic ice cover on marine primary production. *Geophysical Research Letters*, *35*(19), 1–6. https://doi.org/10.1029/2008GL035028

Arrigo, K. R., & van Dijken, G. L. (2015). Continued increases in Arctic Ocean primary production. *Progress in Oceanography*, *136*, 60–70. https://doi.org/10.1016/j.pocean.2015.05.002

Arthun, M., Onarheim, I. H., Dörr, J., & Eldevik, T. (2021). The seasonal and regional transition to an ice-free Arctic. *Geophysical Research Letters*, *48*(1). https://doi.org/10.1029/2020gl090825

Bakker, D. C. E., Pfeil, B., Landa, C. S., Metzl, N., O'Brien, K. M., Olsen, A., et al. (2016). A multi-decade record of high quality fCO_2 data in version 3 of the Surface Ocean CO_2 Atlas (SOCAT). *Earth System Science Data*, *8*, 383–413. https://doi.org/10.5194/essd-8-383-2016

Bates, N. R., Garley, R., Frey, K. E., Shake, K. L., & Mathis, J. T. (2014). Sea-ice melt CO_2–carbonate chemistry in the western Arctic Ocean: Meltwater contributions to air–sea CO_2 gas exchange, mixed-layer properties and rates of net community production under sea ice. *Biogeosciences*, *11*(23), 6769–6789. https://doi.org/10.5194/bg-11-6769-2014

Bates, N. R., & Mathis, J. T. (2009). The Arctic Ocean marine carbon cycle: Evaluation of air-sea CO_2 exchanges, ocean acidification impacts and potential feedbacks. *Biogeosciences*, *6*(11), 2433–2459. https://doi.org/10.5194/bg-6-2433-2009

Bates, N. R., Mathis, J. T., & Jeffries, M. A. (2011). Air-sea CO_2 fluxes on the Bering Sea shelf. *Biogeosciences*, *8*(5), 1237–1253. https://doi.org/10.5194/bg-8-1237-2011

Bates, N. R., Moran, S. B., Hansell, D. A., & Mathis, J. T. (2006). An increasing CO_2 sink in the Arctic Ocean due to sea-ice loss. *Geophysical Research Letters*, *33*, L23609. https://doi.org/10.1029/2006GL027028

Brown, K. A., Holding, J. M., & Carmack, E. C. (2020). Understanding regional and seasonal variability is key to gaining a Pan-Arctic perspective on Arctic Ocean freshening. *Frontiers in Marine Science*, *7*, 606. https://doi.org/10.3389/fmars.2020.00606

Cai, W.-J., Chen, L., Chen, B., Gao, Z., Lee, S. H., Chen, J., et al. (2010). Decrease in the CO_2 uptake capacity in an ice-free Arctic Ocean Basin. *Science*, *329*(5991), 556–559. https://doi.org/10.1126/science.1189338

Cai, W. J., Hu, X., Huang, W. J., Murrell, M. C., Lehrter, J. C., Lohrenz, S. E., et al. (2011). Acidification of subsurface coastal waters enhanced by eutrophication. *Nature Geoscience*, *4*(11), 766–770. https://doi.org/10.1038/ngeo1297

Carter, B. R., Williams, N. L., Evans, W., Fassbender, A. J., Barbero, L., Hauri, C., et al. (2019). Time of detection as a metric for prioritizing between climate observation quality, frequency, and duration. *Geophysical Research Letters*, *46*(7), 3853–3861. https://doi.org/10.1029/2018GL080773

Chen, L., & Gao, Z. (2007). Spatial variability in the partial pressures of CO_2 in the northern Bering and Chukchi seas. *Deep-Sea Research Part II: Topical Studies in Oceanography*, *54*(23–26), 2619–2629. https://doi.org/10.1016/j.dsr2.2007.08.010

Coachman, L. K. (1986). Circulation, water masses, and fluxes on the southeastern Bering Sea shelf. *Continental Shelf Research*, *5*(1–2), 23–108. https://doi.org/10.1016/0278-4343(86)90011-7

Crawford, A. D., Krumhardt, K. M., Lovenduski, N. S., van Dijken, G. L., & Arrigo, K. R. (2020). Summer high-wind events and phytoplankton productivity in the Arctic Ocean. *Journal of Geophysical Research: Oceans*, *125*(9), 1–17. https://doi.org/10.1029/2020JC016565

Creamean, J. M., Cross, J. N., Pickart, R., McRaven, L., Lin, P., Pacini, A., et al. (2019). Ice nucleating particles carried from below a phytoplankton bloom to the Arctic atmosphere. *Geophysical Research Letters*, *46*(14), 8572–8581. https://doi.org/10.1029/2019GL083039

Cross, J., Mathis, J., Frey, K., Cosca, C., Danielson, S., Bates, N., et al. (2014). Annual sea-air CO_2 fluxes in the Bering Sea: Insights from new autumn and winter observations of a seasonally ice-covered continental. *Journal of Geophysical Research: Oceans*, *119*, 6693–6708. https://doi.org/10.1002/2013JC009579

Cross, J. N., Mathis, J. T., Bates, N. R., & Byrne, R. H. (2013). Conservative and non-conservative variations of total alkalinity on the southeastern Bering Sea shelf. *Marine Chemistry*, *154*, 100–112. https://doi.org/10.1016/j.marchem.2013.05.012

Cross, J. N., Mathis, J. T., Lomas, M. W., Moran, S. B., Baumann, M. S., Shull, D. H., et al. (2014). Integrated assessment of the carbon budget in the southeastern Bering Sea. *Deep-Sea Research Part II: Topical Studies in Oceanography*, *109*, 112–124. https://doi.org/10.1016/j.dsr2.2014.03.003

Cross, J. N., Mathis, J. T., Pickart, R. S., & Bates, N. R. (2018). Formation and transport of corrosive water in the Pacific Arctic region. *Deep-Sea Research Part II: Topical Studies in Oceanography*, *152*, 67–81. https://doi.org/10.1016/j.dsr2.2018.05.020

Danielson, S. L., Ahkinga, O., Ashjian, C., Basyuk, E., Cooper, L. W., Eisner, L., et al. (2020). Manifestation and consequences of warming and altered heat fluxes over the Bering and Chukchi Sea continental shelves. *Deep-Sea Research Part II: Topical Studies in Oceanography*, *177*, 104781. https://doi.org/10.1016/j.dsr2.2020.104781

DeGrandpre, M., Evans, W., Timmermans, M. L., Krishfield, R., Williams, B., & Steele, M. (2020). Changes in the Arctic Ocean carbon cycle with diminishing ice cover. *Geophysical Research Letters*, *47*(12). https://doi.org/10.1029/2020GL088051

D'Olivo, J. P., McCulloch, M. T., & Judd, K. (2013). Long-term records of coral calcification across the central Great Barrier Reef: Assessing the impacts of river runoff and climate change. *Coral Reefs*, *32*(4), 999–1012. https://doi.org/10.1007/s00338-013-1071-8

Donlon, C. J., Martin, M., Stark, J., Roberts-Jones, J., Fiedler, E., & Wimmer, W. (2012). The operational sea surface temperature and sea ice analysis (OSTIA) system. *Remote Sensing of Environment*, *116*, 140–158. https://doi.org/10.1016/j.rse.2010.10.017

Duffy-Anderson, J. T., Stabeno, P., Andrews, A. G., Cieciel, K., Deary, A., Farley, E., et al. (2019). Responses of the northern Bering Sea and southeastern Bering Sea Pelagic ecosystems following record-breaking low winter sea ice. *Geophysical Research Letters*, *46*(16), 9833–9842. https://doi.org/10.1029/2019GL083396

ETOPO2. (2006). 2-minute gridded global relief data (ETOPO2v2). National Geophysical Data Center, National Oceanic and Atmospheric Administration, US Department Of commerce. Retrieved from http://www.ngdc.noaa.gov/mgg/global/global.html

Evans, W., Mathis, J. T., & Cross, J. N. (2014). Calcium carbonate corrosivity in an Alaskan inland sea. *Biogeosciences*, *11*(2), 365–379. https://doi.org/10.5194/bg-11-365-2014

Evans, W., Mathis, J. T., Cross, J. N., Bates, N. R., Frey, K. E., Else, B. G. T., et al. (2015). Sea-air CO_2 exchange in the western Arctic coastal ocean. *Global Biogeochemical Cycles*, *29*, 1190–1209. https://doi.org/10.1002/2015GB005153

Fay, A. R., & McKinley, G. A. (2013). Global trends in surface ocean pCO2 from in situ data. *Global Biogeochemical Cycles*, *27*(2), 541–557. https://doi.org/10.1002/gbc.20051

Feely, R. A., Sabine, C. L., Hernandez-Ayon, J. M., Ianson, D., & Hales, B. (2008). Evidence for upwelling of corrosive "acidified" water onto the continental shelf. *Science*, *320*(5882), 1490–1492. https://doi.org/10.1126/science.1155676

Frey, K. E., Moore, G. W. K., Cooper, L. W., & Grebmeier, J. M. (2015). Divergent patterns of recent sea ice cover across the Bering, Chukchi, and Beaufort seas of the Pacific Arctic region. *Progress in Oceanography*, *136*, 32–49. https://doi.org/10.1016/j.pocean.2015.05.009

Geilfus, N.-X., Carnat, G., Dieckmann, G. S., Halden, N., Nehrke, G., Papakyriakou, T., et al. (2013). First estimates of the contribution of $CaCO_3$ precipitation to the release of CO_2 to the atmosphere during young sea ice growth. *Journal of Geophysical Research: Oceans*, *118*, 244–255. https://doi.org/10.1029/2012JC007980

Gong, D., & Pickart, R. S. (2015). Summertime circulation in the eastern Chukchi sea. *Deep Sea Research Part II: Topical Studies in Oceanography*, *118*, 18–31. https://doi.org/10.1016/J.DSR2.2015.02.006

Grebmeier, J. M., Bluhm, B. A., Cooper, L. W., Danielson, S. L., Arrigo, K. R., Blanchard, A. L., et al. (2015). Ecosystem characteristics and processes facilitating persistent macrobenthic biomass hotspots and associated benthivory in the Pacific Arctic. *Progress in Oceanography*, *136*, 92–114. https://doi.org/10.1016/j.pocean.2015.05.006

Itoh, M., Pickart, R. S., Kikuchi, T., Fukamachi, Y., Ohshima, K. I., Simizu, D., et al. (2015). Water properties, heat and volume fluxes of Pacific water in Barrow Canyon during summer 2010. *Deep Sea Research Part I: Oceanographic Research Papers*, *102*, 43–54. https://doi.org/10.1016/j.dsr.2015.04.004

Jones, E. M., Fenton, M., Meredith, M. P., Clargo, N. M., Ossebaar, S., Ducklow, H. W., et al. (2017). Ocean acidification and calcium carbonate saturation states in the coastal zone of the West Antarctic Peninsula. *Deep-Sea Research Part II: Topical Studies in Oceanography*, *139*, 181–194. https://doi.org/10.1016/j.dsr2.2017.01.007

Juranek, L., Takahashi, T., Mathis, J., & Pickart, R. (2019). Significant biologically mediated CO_2 uptake in the Pacific Arctic during the late open water season. *Journal of Geophysical Research: Oceans*, *124*(2), 821–843. https://doi.org/10.1029/2018JC014568

Kachel, N. B., Hunt, G. L., Salo, S. A., Schumacher, J. D., Stabeno, P. J., & Whitledge, T. E. (2002). Characteristics and variability of the inner front of the southeastern Bering Sea. *Deep-Sea Research Part II: Topical Studies in Oceanography*, *49*(26), 5889–5909. https://doi.org/10.1016/S0967-0645(02)00324-7

Kelley, J., Longerich, L., & Hood, D. (1971). Effect of upwelling, mixing, and high primary productivity on CO_2 concentrations in surface waters of the Bering Sea. *Journal of Geophysical Research*, *76*(36), 8687–8693. https://doi.org/10.1029/JC076i036p08687

Ladd, C., & Stabeno, P. J. (2012). Stratification on the eastern Bering Sea shelf revisited. *Deep-Sea Research Part II: Topical Studies in Oceanography*, *65–70*, 72–83. https://doi.org/10.1016/j.dsr2.2012.02.009

Lannuzel, D., Tedesco, L., van Leeuwe, M., Campbell, K., Flores, H., Delille, B., et al. (2020). The future of Arctic sea-ice biogeochemistry and ice-associated ecosystems. *Nature Climate Change*, *10*, 983–992. https://doi.org/10.1038/s41558-020-00940-4

Lewis, K. M., van Dijken, G. L., & Arrigo, K. R. (2020). Changes in phytoplankton concentration now drive increased Arctic Ocean primary production. *Science*, *369*(6500), 198–202. https://doi.org/10.1126/science.aay8380

Lin, P., Pickart, R. S., Fissel, D., Ross, E., Kasper, J., Bahr, F., et al. (2020). Circulation in the vicinity of Mackenzie Canyon from a year-long mooring array. *Progress in Oceanography*, *187*, 102396. https://doi.org/10.1016/j.pocean.2020.102396

Lin, P., Pickart, R. S., McRaven, L. T., Arrigo, K. R., Bahr, F., Lowry, K. E., et al. (2019). Water mass evolution and circulation of the northeastern Chukchi sea in summer: Implications for nutrient distributions. *Journal of Geophysical Research: Oceans*, *124*(7), 4416–4432. https://doi.org/10.1029/2019JC015185

Lin, P., Pickart, R. S., Moore, G. W. K., Spall, M. A., & Hu, J. (2019). Characteristics and dynamics of wind-driven upwelling in the Alaskan Beaufort Sea based on six years of mooring data. *Deep-Sea Research Part II: Topical Studies in Oceanography*, *162*, 79–92. https://doi.org/10.1016/j.dsr2.2018.01.002

Linders, J., Pickart, R. S., Björk, G., & Moore, G. W. K. (2017). On the nature and origin of water masses in Herald Canyon, Chukchi Sea: Synoptic surveys in summer 2004, 2008, and 2009. *Progress in Oceanography*, *159*, 99–114. https://doi.org/10.1016/j.pocean.2017.09.005

Lomas, M. W., Eisner, L. B., Gann, J., Baer, S. E., Mordy, C. W., & Stabeno, P. J. (2020). Time-series of direct primary production and phytoplankton biomass in the southeastern Bering sea: Responses to cold and warm stanzas. *Marine Ecology Progress Series*, *642*, 39–54. https://doi.org/10.3354/meps13317

Lomas, M. W., Moran, S. B., Casey, J. R., Bell, D. W., Tiahlo, M., Whitefield, J., et al. (2012). Spatial and seasonal variability of primary production on the Eastern Bering Sea shelf. *Deep-Sea Research Part II: Topical Studies in Oceanography*, *65–70*, 126–140. https://doi.org/10.1016/j.dsr2.2012.02.010

Manizza, M., Menemenlis, D., Zhang, H., & Miller, C. E. (2019). Modeling the recent changes in the Arctic Ocean CO2 sink (2006–2013). *Global Biogeochemical Cycles*, *33*(3), 420–438. https://doi.org/10.1029/2018GB006070

Mathis, J. T., Bates, N. R., Hansell, D. A., & Babila, T. (2009). Net community production in the northeastern Chukchi Sea. *Deep-Sea Research Part II: Topical Studies in Oceanography*, *56*(17), 1213–1222. https://doi.org/10.1016/j.dsr2.2008.10.017

Mathis, J. T., Cross, J. N., & Bates, N. R. (2011a). Coupling primary production and terrestrial runoff to ocean acidification and carbonate mineral suppression in the eastern Bering Sea. *Journal of Geophysical Research*, *116*, C02030. https://doi.org/10.1029/2010JC006453

Mathis, J. T., Cross, J. N., & Bates, N. R. (2011b). The role of ocean acidification in systemic carbonate mineral suppression in the Bering Sea. *Geophysical Research Letters*, *38*, L19602. https://doi.org/10.1029/2011GL048884

Mathis, J. T., Cross, J. N., Monacci, N., Feely, R. A., & Stabeno, P. (2014). Evidence of prolonged aragonite undersaturations in the bottom waters of the southern Bering Sea shelf from autonomous sensors. *Deep-Sea Research Part II: Topical Studies in Oceanography*, *109*, 125–133. https://doi.org/10.1016/j.dsr2.2013.07.019

Mordy, C. W., Bell, S., Cokelet, E. D., Ladd, C., Lebon, G., Proctor, P., et al. (2020). Seasonal and interannual variability of nitrate in the eastern Chukchi Sea: Transport and winter replenishment. *Deep-Sea Research Part II: Topical Studies in Oceanography*, *177*, 104807. https://doi.org/10.1016/j.dsr2.2020.104807

Mordy, C. W., Cokelet, E. D., Ladd, C., Menzia, F. A., Proctor, P., Stabeno, P. J., et al. (2012). Net community production on the middle shelf of the eastern Bering Sea. *Deep-Sea Research Part II: Topical Studies in Oceanography*, *65–70*, 110–125. https://doi.org/10.1016/j.dsr2.2012.02.012

O'Daly, S. H., Danielson, S. L., Hardy, S. M., Hopcroft, R. R., Lalande, C., Stockwell, D. A., et al. (2020). Extraordinary carbon fluxes on the shallow Pacific Arctic shelf during a remarkably warm and low sea ice period. *Frontiers in Marine Science*, *7*, 548931. https://doi.org/10.3389/fmars.2020.548931

Orr, J. C., Fabry, V. J., Aumont, O., Bopp, L., Doney, S. C., Feely, R. A., et al. (2005). Anthropogenic ocean acidification over the twenty-first century and its impact on calcifying organisms. *Nature*, *437*(7059), 681–686. https://doi.org/10.1038/nature04095

Ouyang, Z., Qi, D., Chen, L., Takahashi, T., Zhong, W., DeGrandpre, M. D., et al. (2020). Sea-ice loss amplifies summertime decadal CO_2 increase in the western Arctic Ocean. *Nature Climate Change*, *10*(7), 678–684. https://doi.org/10.1038/s41558-020-0784-2

Ouyang, Z., Qi, D., Zhong, W., Chen, L., Gao, Z., Lin, H., et al. (2021). Summertime evolution of net community production and CO_2 flux in the western Arctic Ocean. *Global Biogeochemical Cycles*, *35*, e2020GB006651. https://doi.org/10.1029/2020GB006651

Pickart, R. S., Moore, G., Mao, C., Bahr, F., Nobre, C., & Weingartner, T. J. (2016). Circulation of winter water on the Chukchi shelf in early Summer. *Deep Sea Research Part II: Topical Studies in Oceanography*, *130*, 56–75. https://doi.org/10.1016/j.dsr2.2016.05.001

Pickart, R. S., Nobre, C., Lin, P., Arrigo, K. R., Ashjian, C. J., Berchok, C., et al. (2019). Seasonal to mesoscale variability of water masses and atmospheric conditions in Barrow Canyon, Chukchi Sea. *Deep-Sea Research Part II: Topical Studies in Oceanography*, *162*, 32–49. https://doi.org/10.1016/j.dsr2.2019.02.003

Pilcher, D. J., Siedlecki, S. A., Hermann, A. J., Coyle, K. O., Mathis, J. T., & Evans, W. (2018). Simulated impact of glacial runoff on CO_2 uptake in the Gulf of Alaska. *Geophysical Research Letters*, *45*(2), 880–890. https://doi.org/10.1002/2017GL075910

Polukhin, A. (2019). The role of river runoff in the Kara Sea surface layer acidification and carbonate system changes. *Environmental Research Letters*, *14*(10). https://doi.org/10.1088/1748-9326/ab421e

Qi, D., Chen, L., Chen, B., Gao, Z., Zhong, W., Feely, R. A., et al. (2017). Increase in acidifying water in the western Arctic Ocean. *Nature Climate Change*, *7*, 195–199. https://doi.org/10.1038/nclimate3228

Reynolds, R. W., Smith, T. M., Liu, C., Chelton, D. B., Casey, K. S., & Schlax, M. G. (2007). Daily high-resolution-blended analyses for sea surface temperature. *Journal of Climate*, *20*(22), 5473–5496. https://doi.org/10.1175/2007JCLI1824.1

Rysgaard, S., Bendtsen, J., Delille, B., Dieckmann, G. S., Glud, R. N., Kennedy, H., et al. (2011). Sea ice contribution to the air–sea CO_2 exchange in the Arctic and Southern Oceans. *Tellus B: Chemical and Physical Meteorology*, *63*(5), 823–830. https://doi.org/10.1111/j.1600-0889.2011.00571.x

Rysgaard, S., Bendtsen, J., Pedersen, L. T., Ramtøv, H., & Glud, R. N. (2009). Increased CO_2 uptake due to sea ice growth and decay in the Nordic Seas. *Journal of Geophysical Research*, *114*, C09011. https://doi.org/10.1029/2008JC005088

Rysgaard, S., Glud, R. N., Sejr, M. K., Bendtsen, J., & Christensen, P. B. (2007). Inorganic carbon transport during sea ice growth and decay: A carbon pump in polar seas. *Journal of Geophysical Research*, *112*(C3). https://doi.org/10.1029/2006JC003572

Sabine, C., Sutton, A., McCabe, K., Lawrence-Slavas, N., Alin, S., Feely, R., et al. (2020). Evaluation of a new carbon dioxide system for autonomous surface vehicles. *Journal of Atmospheric and Oceanic Technology*, *37*(8), 1305–1317. https://doi.org/10.1175/JTECH-D-20-0010.1

Schumacher, J., Kinder, T. H., Pashinski, D. J., & Charnell, R. L. (1979). A Structural front over the continental shelf of the eastern Bering Sea. *Journal of Physical Oceanography*, 79–87. https://doi.org/10.1175/1520-0485(1979)009<0079:asfotc>2.0.co;2

Schuur, E. A. G., McGuire, A. D., Schädel, C., Grosse, G., Harden, J. W., Hayes, D. J., et al. (2015). Climate change and the permafrost carbon feedback. *Nature*, *520*(7546), 171–179. https://doi.org/10.1038/nature14338

Sigler, M. F., Mueter, F. J., Bluhm, B. A., Busby, M. S., Cokelet, E. D., Danielson, S. L., et al. (2017). Late summer zoogeography of the northern Bering and Chukchi seas. *Deep Sea Research Part II: Topical Studies in Oceanography*, *135*, 168–189. https://doi.org/10.1016/j.dsr2.2016.03.005

Sigler, M. F., Stabeno, P. J., Eisner, L. B., Napp, J. M., & Mueter, F. J. (2014). Spring and fall phytoplankton blooms in a productive subarctic ecosystem, the eastern Bering Sea, during 1995–2011. *Deep-Sea Research Part II: Topical Studies in Oceanography*, *109*, 71–83. https://doi.org/10.1016/j.dsr2.2013.12.007

Stabeno, P., Kachel, N., Ladd, C., & Woodgate, R. (2018). Flow patterns in the eastern Chukchi sea: 2010–2015. *Journal of Geophysical Research: Oceans*, *123*(2), 1177–1195. https://doi.org/10.1002/2017JC013135

Stabeno, P. J., Bell, S. W., Bond, N. A., Kimmel, D. G., Mordy, C. W., & Sullivan, M. E. (2019). Distributed biological observatory region 1: Physics, chemistry and plankton in the northern Bering Sea. *Deep-Sea Research Part II: Topical Studies in Oceanography*, *162*, 8–21. https://doi.org/10.1016/j.dsr2.2018.11.006

Stabeno, P. J., Danielson, S. L., Kachel, D. G., Kachel, N. B., & Mordy, C. W. (2016). Currents and transport on the Eastern Bering Sea shelf: An integration of over 20 years of data. *Deep-Sea Research Part II: Topical Studies in Oceanography*, *134*, 13–29. https://doi.org/10.1016/j.dsr2.2016.05.010

Stabeno, P. J., Reed, R. K., & Schumacher, J. D. (1995). The Alaska coastal current: Continuity of transport and forcing. *Journal of Geophysical Research*, *100*(C2), 2477–2485. https://doi.org/10.1029/94JC02842

Stabeno, P. J., Schumacher, J. D., & Ohtani, K. (1999). The physical oceanography of the Bering Sea. In T. R. Loughlin & K. Ohtani (Eds.), *Dynamics of the Bering Sea: A Summary of physical, chemical, and biological characteristics, and a synopsis of research on the Bering Sea*. Alaska sea grant (pp. 1–28).

Sun, H., Gao, Z., Qi, D., Chen, B. S., Chen, L., & Cai, W. J. (2020). Surface seawater partial pressure of CO_2 variability and air-sea CO_2 fluxes in the Bering Sea in July 2010. *Continental Shelf Research*, *193*, 104031. https://doi.org/10.1016/j.csr.2019.104031

Sutton, A. J., Feely, R. A., Maenner-Jones, S., Musielwicz, S., Osborne, J., Dietrich, C., et al. (2019). Autonomous seawater pCO_2 and pH time series from 40 surface buoys and the emergence of anthropogenic trends. *Earth System Science Data*, *11*(1), 421–439. https://doi.org/10.5194/essd-11-421-2019

Takahashi, T., Sutherland, S. C., Chipman, D. W., Goddard, J. G., Ho, C., Newberger, T., et al. (2014). Climatological distributions of pH, pCO_2, total CO_2, alkalinity, and $CaCO_3$ saturation in the global surface ocean, and temporal changes at selected locations. *Marine Chemistry*, *164*, 95–125. https://doi.org/10.1016/j.marchem.2014.06.004

Takahashi, T., Sutherland, S. C., Sweeney, C., Poisson, A., Metzl, N., Tilbrook, B., et al. (2002). Global sea-air CO_2 flux based on climatological surface ocean pCO_2, and seasonal biological and temperature effects. *Deep-Sea Research Part II: Topical Studies in Oceanography*, *49*(9–10), 1601–1622. https://doi.org/10.1016/S0967-0645(02)00003-6

Takahashi, T., Sutherland, S. C., Wanninkhof, R., Sweeney, C., Feely, R. A., Chipman, D. W., et al. (2009). Climatological mean and decadal change in surface ocean pCO_2, and net sea-air CO_2 flux over the global oceans. *Deep-Sea Research Part II: Topical Studies in Oceanography*, *56*(8–10), 554–577. https://doi.org/10.1016/j.dsr2.2008.12.009

Tank, S. E., Striegl, R. G., McClelland, J. W., & Kokelj, S. V. (2016). Multi-decadal increases in dissolved organic carbon and alkalinity flux from the Mackenzie drainage basin to the Arctic Ocean. *Environmental Research Letters*, *11*(5), 054015. https://doi.org/10.1088/1748-9326/11/5/054015

Terhaar, J., Kwiatkowski, L., & Bopp, L. (2020). Emergent constraint on Arctic Ocean acidification in the twenty-first century. *Nature*, *582*, 379–383. https://doi.org/10.1038/s41586-020-2360-3

Tian, F., Pickart, R. S., Lin, P., Pacini, A., Moore, G. W. K., Stabeno, P., et al. (2021). Mean and seasonal circulation of the eastern Chukchi sea from moored timeseries in 2013–2014. *Journal of Geophysical Research: Oceans*, *126*(5), e2020JC016863. https://doi.org/10.1029/2020jc016863

Timmermans, M. L., Toole, J., & Krishfield, R. (2018). Warming of the interior Arctic Ocean linked to sea ice losses at the basin margins. *Science Advances*, *4*(8), 1–7. https://doi.org/10.1126/sciadv.aat6773

Titchner, H. A., & Rayner, N. A. (2014). The Met Office Hadley Centre Sea ice and sea surface temperature data set, version 2: 1. Sea ice concentrations. *Journal of Geophysical Research: Atmospheres*, *119*(6), 2864–2889. https://doi.org/10.1002/2013jd020316

Vonk, J. E., Tank, S. E., Bowden, W. B., Laurion, I., Vincent, W. F., Alekseychik, P., et al. (2015). Reviews and syntheses: Effects of permafrost thaw on Arctic aquatic ecosystems. *Biogeosciences*, *12*(23), 7129–7167. https://doi.org/10.5194/bg-12-7129-2015

Waga, H., & Hirawake, T. (2020). Changing occurrences of fall Blooms associated with variations in phytoplankton size structure in the Pacific Arctic. *Frontiers in Marine Science*, *7*, 209. https://doi.org/10.3389/fmars.2020.00209

Walvoord, M. A., & Striegl, R. G. (2007). Increased groundwater to stream discharge from permafrost thawing in the Yukon River basin: Potential impacts on lateral export of carbon and nitrogen. *Geophysical Research Letters*, *34*(12). https://doi.org/10.1029/2007GL030216

Wanninkhof, R. (2014). Relationship between wind speed and gas exchange over the ocean revisited. *Limnology and Oceanography: Methods*, *12*, 351–362. https://doi.org/10.4319/lom.2014.12.351

Ward, C. P., Nalven, S. G., Crump, B. C., Kling, G. W., & Cory, R. M. (2017). Photochemical alteration of organic carbon draining permafrost soils shifts microbial metabolic pathways and stimulates respiration. *Nature Communications*, *8*(1), 1–7. https://doi.org/10.1038/s41467-017-00759-2

Ward, C. P., Sleighter, R. L., Hatcher, P. G., & Cory, R. M. (2014). Insights into the complete and partial photooxidation of black carbon in surface waters. *Environmental Sciences: Processes and Impacts*, *16*(4), 721–731. https://doi.org/10.1039/c3em00597f

Weingartner, T. J., Danielson, S., Sasaki, Y., Pavlov, V., & Kulakov, M. (1999). The Siberian coastal current: A wind- and buoyancy-forced Arctic coastal current. *Journal of Geophysical Research*, *104*(C12), 29697–29713. https://doi.org/10.1029/1999jc900161

Woodgate, A. R., & Peralta-Ferriz, C. (2021). Warming and freshening of the Pacific inflow to the Arctic from 1990-2019 implying dramatic Shoaling in Pacific winter water ventilation of the Arctic water column. *Geophysical Research Letters*, *48*(9), e2021GL092528. https://doi.org/10.1029/2021GL092528

Woodgate, R. A. (2018). Increases in the Pacific inflow to the Arctic from 1990 to 2015, and insights into seasonal trends and driving mechanisms from year-round Bering Strait mooring data. *Progress in Oceanography*, *160*, 124–154. https://doi.org/10.1016/j.pocean.2017.12.007

Woodgate, R. A., Aagaard, K., & Weingartner, T. J. (2005). Monthly temperature, salinity, and transport variability of the Bering Strait through flow. *Geophysical Research Letters*, *32*(4), 1. https://doi.org/10.1029/2004GL021880

Woodgate, R. A., Stafford, K. M., & Prahl, F. G. (2015). A synthesis of year-round interdisciplinary mooring measurements in Russian-American long-term census of the Arctic a synthesis of year-round interdisciplinary mooring measurements in the Bering Strait (1990–2014) and the RUSALCA years (2004–2011). *Oceanography*, *28*(3), 46–67. https://doi.org/10.5670/oceanog.2015.57

Woosley, R. J., & Millero, F. J. (2020). Freshening of the western Arctic negates anthropogenic carbon uptake potential. *Limnology and Oceanography*, *65*(8), 1834–1846. https://doi.org/10.1002/lno.11421